

Review

# Non-Platinum Metal Complexes as Potential Anti-Triple Negative Breast Cancer Agents

Eva María Domínguez-Martís <sup>1</sup>, Diego Gabriel Mosteiro-Miguéns <sup>2</sup>, Lucía Vigo-Gendre <sup>1</sup>, David López-Ares <sup>3</sup>, Manuel Freire-Garabal <sup>4</sup>, María Jesús Núñez-Iglesias <sup>4</sup> and Silvia Novío <sup>4,\*</sup> 

<sup>1</sup> Galician Public Health Care Service, Health Care Centre of Ordes, C/Ramón Ferreiro s/n, 15680 Ordes, A Coruña, Spain; eva.dominguez2@hotmail.com (E.M.D.-M.); lucia.vigo.gendre@gmail.com (L.V.-G.)

<sup>2</sup> Badalona Serveis Assistencials, Family and Community Nursing, Health Care Centre of Morera-Pomar, C/PERE III, N° 1-7, 08915 Badalona, Barcelona, Spain; diegomoste@gmail.com

<sup>3</sup> Galician Public Health Care Service, University Hospital Complex of A Coruña (CHUAC), C/Xubias de Arriba, 84, 15006 A Coruña, Spain; dlopaes@gmail.com

<sup>4</sup> SNL Laboratory, School of Medicine and Dentistry, University of Santiago de Compostela, C/San Francisco s/n, 15782 A Coruña, Spain; mjesus.nunez@usc.es (M.F.-G.); manuel.freire-garabal@usc.es (M.J.N.-I.)

\* Correspondence: silvia.novio@usc.es; Tel.: +34-881812374

Received: 12 August 2018; Accepted: 18 September 2018; Published: 20 September 2018



**Abstract:** Breast cancer (BC) is the most common cancer in women worldwide, with a mortality rate that has been forecasted to rise in the next decade. This is especially worrying for people with triple-negative BC (TNBC), because of its unresponsiveness to current therapies. Different drugs to treat TNBC have been assessed, and, although platinum chemotherapy drugs seem to offer some hope, their drawbacks have motivated extensive investigations into alternative metal-based BC therapies. This paper aims to: (i) describe the preliminary in vitro and in vivo anticancer properties of non-platinum metal-based complexes (NPMBC) against TNBC; and (ii) analyze the likely molecular targets involved in their anticancer activity.

**Keywords:** antiproliferative activity; apoptosis; metal complexes; metastasis; treatment; triple negative breast cancer

## 1. Introduction

Breast cancer (BC) is, despite therapeutic advances, the most common cancer among females (1.5 million women worldwide each year) and the leading cause of death from cancer in women (570,000 in 2015). Furthermore, its incidence is expected to rise in the coming decades [1]. This global increase in the BC burden is mainly attributed to exogenous factors such as reproductive and lifestyle factors; however, genetic risk factors such as mutations in breast cancer susceptibility gene 1 (BRCA1) and gene 2 (BRCA2), which are associated to tumors with more aggressive phenotypes, play an important role in the etiology of this type of cancer [2,3].

BC is classified according to the expression of immunohistochemical markers in luminal A, luminal B, HER-2 positive and triple negative subtypes, being the triple negative subtype further divided into A (luminal-like) and B (basal-like) [4,5] (Table 1). The basal-like cancers account for 60–90% of triple negative cases, with the BC subtype having the worst prognosis. Compared with the other subtypes, triple negative breast cancer (TNBC) is more likely to be diagnosed at a younger age; it is more frequently associated with mutations in the BRCA; it usually has rapid growth and large size; it frequently overexpresses genes involved in drug-desensitizing mechanisms (for example, ABCC1 or MRP1 (multidrug resistance protein 1)); and it has a high rate of early recurrence and of distant metastasis (brain, lung, bone, and liver), and a low disease-specific survival [6]. Furthermore, due to

the lack of specific molecular targets in this subtype of BC [7], which makes its treatment difficult, chemotherapy remains an essential component for the management of TNBC, both adjuvant and neoadjuvant therapy [8,9].

**Table 1.** Characterization of the main triple negative breast cancer (TNBC) cell lines according to the subtype and molecular features.

Subtype	TNBC Cell Lines	Others Immunohistochemical Markers besides ER, PR and HER2 <sup>a</sup>	Tumor of Origin
A	BT-20	WNT3 oncogene +, WNT7B oncogene +	Invasive ductal carcinoma
	CAL148	CK 7 +, CK 8 +, CK 17 – CK 18 +, CK 19 +, desmin –, endothel –, EpCAM +, GFAP –, neurofilament –, vimentin –	Adenocarcinoma
	DU4475	CK 7 –, CK 8 +, CK 17 –, CK 18 +, CK 19 –, desmin –, endothel –, EpCAM +, GFAP –, neurofilament –, vimentin –	Invasive ductal carcinoma
	EMG3	CK 5 +, CK 14 +, CK 18 +, CK 19 –, EMA +, P63+, SMA –, ESA +, EGFR +	Invasive ductal carcinoma
	HCC1143	p53 +, EGP2 +, CK 19 +	Ductal carcinoma
	HCC1187	EGP2 +, CK 19 +, p53 +++	Ductal carcinoma
	HCC1599	EGP2 +, CK 19 +, p53 –	Ductal carcinoma
	HCC1806	p53 –, EGP2 +, CK 19 +, Ob-R +	Squamous carcinoma
	HCC1937	p53 –, EGP2 +, CK 19 +	Ductal carcinoma
	HCC2157	EGP2 +, CK 19 +, p53 +	Ductal carcinoma
	HCC3153	N.A.	Ductal carcinoma
	HCC70	p53 +, EGP2 + CK 19 +	Ductal carcinoma
	HMT3522	Vimentin –, PLK1 +	Benign tumor
	KPL-3C	Keratins –, Vimentin –	Invasive ductal carcinoma
	MA11	e-cadherin +	Invasive lobular carcinoma
	MDA-MB-436	Tubulin +, actin +, ICAM +++	Adenocarcinoma
	MDA-MB-468	EGFR +, TGF alpha +, Ki67 high	Adenocarcinoma
	MFM223	CK 7 +, CK 8 +, CK 17 –, CK 18 +, CK 19 +, desmin –, endothel –, EpCAM +, GFAP –, neurofilament –, vimentin –	Carcinoma
	SUM229PE	CK 8 +, CK 18 +, CK 19 +	Ductal carcinoma
	B	A17	Vimentin +, CK 14 +, N-cadherin +, COX2 +++
BCM-2665A		ALDH +	Invasive ductal carcinoma
BT-549		Ki67 low, e-cadherin low, claudin-3 low, claudinin-4 low, claudinin-7 low	Invasive ductal carcinoma
CAL-120		CK 7 –, CK 8 +, CK 17 –, CK 18 +, CK 19 +, desmin –, endothel –, EpCAM +, GFAP –, neurofilament –, vimentin +	Adenocarcinoma
CAL-51		CK 7 –, CK 8 +, CK 17 –, CK 18 +, CK 19 +, desmin –, endothel –, EpCAM +, GFAP –, neurofilament –, vimentin +	Adenocarcinoma
CAL-85-1		CK 7 +, CK 8 +, CK 17 +, CK 18 +, CK 19 +, desmin –, endothel –, EpCAM +, GFAP –, neurofilament –, vimentin +	Adenocarcinoma
HCC1395		p53 +, EGP2 +, CK 19 +	Ductal carcinoma
HCC1739		N.A.	Ductal carcinoma
HCC38		p53 +, EGP2 +, CK 19 +	Ductal carcinoma
HDQ-P1		CK 7 +, CK 8 +, CK 17 +, CK 18 +, CK 19 +, desmin –, endothel –, EpCAM +, GFAP –, neurofilament –, vimentin +	Invasive ductal carcinoma
Hs578T		Ki67 low, e-cadherin low, claudin-3 low, claudinin-4 low, claudinin-7 low, EGFR +	Invasive ductal carcinoma
MDA-MB-157		WNT7B oncogene +, ICAM +++	Medullary carcinoma
MDA-MB-231		EGFR +, TGF alpha +, CD44 +, LHRH +, WNT7B oncogene +, ICAM-1 +, Ki67 low, e-cadherin low, claudin-3 low, claudinin-4 low, claudinin-7 low, alpha-V beta-3 integrin +, Ob-R +	Adenocarcinoma
OCUB-M		e-cadherin +, Laminin +	Carcinoma
SUM1315		EGFR +	Carcinoma
SUM149		CK 8 +, CK 18 +, CK 19 +	Carcinoma
SUM159		claudin low, CK 8 +, CK 18 +, CK 19 +	Carcinoma

The correspondence between the cell lines and clinical features of the tumor of origin is provided. <sup>a</sup> Estrogen receptors (ER), progesterone receptors (PR) and human epidermal growth factor receptor 2 (HER2) are all negative. Abbreviations: –, Negative; +, Positive; +++, Overexpression; ALDH, Aldehyde Dehydrogenase; CK, Cytokeratin; COX, Cyclooxygenase; EGF, Epidermal Growth Factor; EGFR, Epidermal Growth Factor Receptor; EGP, Epithelial Glycoprotein; EMA, Epithelial Membrane Antigen; EpCAM, Epithelial Cell Adhesion Molecule; ESA, Epithelial Specific Antigen; GFAP, Glial Fibrillary Acidic Protein; ICAM, Intercellular Adhesion Molecule; LHRH, Luteinizing Hormone-Releasing Hormone; N.A., Not Available; Ob-R, Leptin Receptor; PLK, Polo-Like Kinase; SMA, Smooth Muscle Actin; TGF alpha, Transforming growth factor alpha [4,10–13].

Besides their diagnostic use [14–21], metallodrugs or metal-based complexes (MBC) stand out for being promising chemotherapeutic agents [22]. The therapeutic potential of MBC has long been known; however, their role in the treatment of cancer is relatively recent (1960s). The first metal that laid the foundations of the modern era of metal-based anticancer drugs was platinum, and particularly its drug-derived cisplatin of which cytotoxic activity depends on apoptotic mechanisms and DNA repair defects caused by BRCA1 dysfunction [23,24], hence BRCA-deficient TNBC cells are particularly sensitive to it [25]. However, both cisplatin chemotherapies and its analogs have been shown to have major drawbacks (i.e., intrinsic and acquired chemoresistance, high general toxicity and limited spectrum of activity) [26] which have motivated extensive investigations into alternative metal-based cancer therapies that effectively target both cancer cell proliferation and metastasis. In this sense, we can mention chemotherapy with gold compounds [27–46]—because they are nontoxic, nonimmunogenic and have good photothermal and optical properties, biocompatibility and stability [40,47,48]—and also with copper [49–51], ruthenium [16,52–59], iron [56,60–65], palladium [50], silver [66,67], iridium [68], osmium [68] and rhodium [69] compounds.

This paper aims to: (i) describe the preliminary *in vitro* and *in vivo* anticancer properties of non-platinum MBC (NPMBC) against TNBC; and (ii) analyze the likely molecular targets involved in their anticancer activity.

## 2. Anticancer Effects of Non-Platinum MBC (NPMBC)

The mechanisms behind the anticancer effects of NPMBC are not fully understood, but known responses to them include the following: (i) suppression of cancer cell viability (Table 2) in association with induction of cell death (Tables 3 and 4); and (ii) inhibition of metastatic processes (Table 5). Furthermore, a study suggests that NPMBC could also inhibit angiogenesis [55]; however, because of scarce evidence, no definitive conclusion can be drawn on the role of these compounds in the regulation of blood vessel formation. In any case, it is thought that NPMBC are frequently multi-targeted and attack different biochemical pathways simultaneously [53,66,68], sometimes in a synergic way [37,62].

**Table 2.** Non-platinum metal based complexes (NPMBC) inhibit the in vitro and in vivo growth of triple-negative breast cancer (TNBC) cells by inhibiting tumor cell proliferation.

Cell Line	NPMBC	Assay	In Vitro		Doses Assayed	Reference
			Mode of Action/Pathway Involved	Effect Observed		
MDA-MB-231	Multibranched gold nanoantennas	Calcein/PI staining assay	—	Induction of cell death	170 µg/mL	[14]
MDA-MB-231 SUM159 MDA-MB-468 BT-549	Liposome encapsulated ruthenium polypyridine complex	MTT assay	—	Reduced cell viability	<4 µM	[16]
MDA-MB-231	Liposome encapsulated ruthenium polypyridine complex	Western blot Immunofluorescence	γ-H2AX ATM	Increased levels of γ-H2AX Degradation and dephosphorylation of ATM	3 µM	[16]
MDA-MB-231	Gold nanostars loaded with AS1411	Resazurin cell viability assay	—	40% cell viability	0.3 nM	[27]
MDA-MB-231	CD44-targeting HSP72 depletion nanosystem based on plasmonic gold nanoparticles	MTT assay	—	20–85% cell death	50 mg/L	[28]
MDA-MB-231	Multibranched gold nanoantennas	MTT assay	—	~40% cell viability	170 µg/mL	[29]
MDA-MB-231	Gold nanoparticles	MTT assay	—	15–75% survival	0.1–100 µM	[31]
MDA-MB-231	Thioglucose-bound gold nanoparticles	MTT assay	—	Inhibited cell growth	20 nM	[36]
MDA-MB-231	Thioglucose-bound gold nanoparticles	Clonogenic cell survival assay	—	Enhanced radiosensitivity	20 nM	[36]
MDA-MB-231 MDA-MB-468	Anti-EGFR-gold nanorod conjugates	MTT assay	—	Inhibited cell growth	1.84 µg/mL	[37]
MDA-MB-231	Anti-EGFR-gold nanorod conjugates	Western blot	Ki-67 EGFR Akt ERK1/2 mTOR FAK	Decreased Ki-67 and EGFR expression Suppression of phosphorylation of FAK, ERK1/2, mTOR and Akt	1.84 µg/mL	[37]
MDA-MB-231	Anti-EGFR-gold nanorod conjugates	CCK-8 assay	—	32.2% cell viability	120 pM	[38]
MDA-MB-231	Gold nanospheres conjugated with AS1411	MTT assay	—	Inhibited cell viability	<100 nM	[39]
MDA-MB-231 SUM1315 HCC1937 MDA-MB-468	Gold-nanoparticles conjugated with Rad6 inhibitor	MTT assay Trypan blue staining assay	—	Decreased cell viability (SUM1315 and MDA-MB-231) No change in viability of HCC1937 and MDA-MB-468	0.5 µM for SUM1315; 8.2 µM for MDA-MB-231	[40]

Table 2. Cont.

Cell Line	NPMBC	Assay	In Vitro			Reference
			Mode of Action/Pathway Involved	Effect Observed	Doses Assayed	
MDA-MB-231	Gold nanoparticles loaded with 5-fluorouracil	MTT assay	—	Decreased cell viability	0.5 nM	[41]
MDA-MB-231	Chitosan layered gold nanorods	MTS-based colorimetric assay	—	~65% inhibition of cell proliferation	100 nM	[43]
MDA-MB-231 MDA-MB-468	Micellar gold nanoparticles conjugated with ZD6474	MTT assay	—	80.51% (MDA-MB-231) and ~92% (MDA-MB-468) inhibition of cell proliferation	1–10 $\mu$ M	[44]
MDA-MB-231 BT-20	Copper salicylate phenanthroline complexes	MTS-based colorimetric assay	—	Inhibition of cell growth	5–25 $\mu$ M	[49]
MDA-MB-231	Copper complexes of phenanthrenequinone thiosemicarbazone	MTT assay	—	Decreased cell viability	2.3–4.8 $\mu$ M	[50]
MDA-MB-231	Nickel complexes of phenanthrenequinone thiosemicarbazone	MTT assay	—	Decreased cell viability	>10 $\mu$ M	[50]
MDA-MB-231	Palladium complexes of phenanthrenequinone thiosemicarbazone	MTT assay	—	Decreased cell viability	>10 $\mu$ M	[50]
MDA-MB-231	Copper oxide nanowire conjugated with folic acid	Flow cytometry	—	60% cell death	2.5 $\mu$ g/mL	[51]
MDA-MB-231	Water-soluble iminophosphorane ruthenium(II) compounds	MTT assay	—	Decreased cell viability	2.61–75.4 $\mu$ M	[52]
MDA-MB-231 MDA-MB-468 MDA-MB-436	Ruthenium-based nucleolipidic nanoaggregates	MTT assay Trypan blue	—	Reduced cell proliferation	12.1–14.7 $\mu$ M	[53]
MDA-MB-231 HCC1937	Ruthenium complexes	Real-time cell growth profiling MTT assay	—	Inhibited cell viability	13.2 and 14.1 $\mu$ M for MDA-MB-231; 1.8 and 9.9 $\mu$ M for HCC1937	[54]
A17 MDA-MB-231	Ruthenium complexes	MTT assay	—	Inhibited cell viability	230.66 $\mu$ M for A17; 409.89 $\mu$ M for MDA-MB-231	[55]
MDA-MB-231	Ansa-ferrocenes ruthenocenophanes	MTT assay	—	Decreased cell viability	0.09–4.53 $\mu$ M	[56]
MDA-MB-231	Ruthenium(II) paracyme complexes	Sulforhodamine B assay	—	Decreased cell viability	9.2–29.1 $\mu$ M	[57]
MDA-MB-231	Ruthenium complexes	MTT assay	—	Decreased cell viability	8.81–21.92 $\mu$ M	[58]
MDA-MB-231	Ruthenium complexes	Colony formation	—	100% inhibition of the colony formation	2 $\mu$ M	[58]
MDA-MB-231	Ruthenium-based compounds	MTT assay	—	Decreased cell viability	31.16 and 52.74 $\mu$ M	[59]

Table 2. Cont.

Cell Line	NPMBC	Assay	In Vitro			Reference
			Mode of Action/Pathway Involved	Effect Observed	Doses Assayed	
MDA-MB-231	Ruthenium-based compounds	Colony formation	—	100% inhibition of the colony formation	20 $\mu$ M	[59]
SUM159	Iron oxide nanoparticles	Alamar blue cell viability assay Flow cytometry	—	5–80% cell viability	10 $\mu$ M	[61]
MDA-MB-231	Supermagnetic iron oxide nanoparticles conjugated with doxorubicin	MTS-based colorimetric assay	—	31%-cell viability	520 $\mu$ M	[62]
MDA-MB-231	Chitosan hydrogel cross-linked with telechelic difunctional poly(ethylene glycol) modified iron oxide magnetic nanoparticles	CCK-8 assay	—	5.6% cell viability	10.8–35.8 $\mu$ M	[63]
MDA-MB-231 HCC1806	Iron oxide nanoparticles linked antagonist for leptin	MTT assay	—	Prevention of leptin-induced cell proliferation	0.0036 pmol/L	[64]
MDA-MB-231 HCC1806	Iron oxide nanoparticles linked antagonist for leptin	Immunoblotting analysis	Cyclin D1	Prevention of leptin-induced cyclin D1 expression	0.0036 pmol/L	[64]
MDA-MB-231 HCC1806	Iron oxide nanoparticles linked antagonist for leptin	Cell cycle analysis	—	Prevention of leptin-induced cell cycle progression	0.0018–0.0036 pmol/L for MDA-MB-231 and 0.0018–0.036 pmol/L for HCC1806	[64]
MDA-MB-231 HCC 1806	Iron oxide nanoparticles linked antagonist for leptin	FITC-annexin V/PI staining assay	—	Decreased cell viability	0.0036 pmol/L	[64]
MDA-MB-231	Doxorubicin-hyaluronan conjugated iron oxide nanoparticles	Confocal microscopy	Vimentin e-cadherin	Decreased vimentin expression No change in e-cadherin expression	2 $\mu$ M	[65]
MDA-MB-231 BT549 SUM-159	Silver nanoparticles	MTT assay	—	Inhibited cell viability	$\geq$ 10 $\mu$ g/mL	[66]
MDA-MB-231 BT549 SUM-159	Silver nanoparticles	Clonogenic assay	—	100% inhibition of clonogenic growth	$\geq$ 10 $\mu$ g/mL	[66]
MDA-MB-231	Silver nanoparticles	MTT assay	—	Decreased cell viability	6.72 $\mu$ g/mL at 12 h and 2.62 $\mu$ g/mL at 24 h	[67]
MDA-MB-468 OCUB-M	Organo-iridium complexes Organo-osmium complexes	MTT assay	—	Decreased cell viability	<1 $\mu$ M	[68]
MDA-MB-468 MDA-MB-231	Rhodium(III) complex	MTT assay	—	Inhibited cell proliferation	0.35 and 0.55 $\mu$ M	[69]

Table 2. Cont.

In Vitro						
Cell Line	NPMBC	Assay	Mode of Action/Pathway Involved	Effect Observed	Doses Assayed	Reference
MDA-MB-231	Rhodium(III) complex	Western blot	Wee 1 Cdc2 ERK Akt Cyclin A2 $\gamma$ -H2AX	Decreased phosphorylation of ERK, Akt, Cdc2 Decreased expression of cyclin A2 Increased $\gamma$ -H2AX levels Inhibition of Wee1 activity	1–3 $\mu$ M	[69]
In Vivo						
Cell Line	NPMBC	Animal (Model)/Analysis from Animal Tissue	Mode of Action/Pathway Involved	Effect Observed	Doses Assayed (Route of Administration)	Reference
MDA-MB-231	Liposome encapsulated ruthenium polypyridine complex	Athymic nude mice (orthotopic)/Immunofluorescence imaging	Ki-67	Decreased Ki-67 level	5 mg ruthenium/kg (i.v.)	[16]
MDA-MB-231	Liposome encapsulated ruthenium polypyridine complex	Athymic nude mice (orthotopic)	—	Suppression of tumor growth (tumor weights: 0.342 with nanoparticles vs. 0.992 with control)	5 mg ruthenium/kg (i.v.)	[16]
MDA-MB-231	CD44-targeting HSP72 depletion nanosystem based on plasmonic gold nanoparticles	Nude mice (xenograft)	—	Smaller tumor volume than control	10 mg/kg (i.v.)	[28]
MDA-MB-231	Gold nanomatryoshkas and nanoshells	Sprague-Dawley athymic nude mice (xenograft)	—	Improved survival (15.8 and 11.3 days with nanomatryoshkas and nanoshells respectively) Slower tumor growth with nanomatryoshkas	300 $\mu$ g of gold (i.v.)	[32]
MDA-MB-231	Anti-EGFR-gold nanorod conjugates	BALB/c nude mice (xenograft)	—	Smaller tumor volume than control (~<50 vs. 250 mm <sup>3</sup> respectively)	0.5 pmol/g mouse (i.v.)	[37]
MDA-MB-231	Anti-EGFR-gold nanorod conjugates	BALB/c nude mice (xenograft)/Immunohistochemistry	Ki-67 EGFR	Decreased Ki-67 and EGFR levels	0.5 pmol/g mouse (i.v.)	[37]
MDA-MB-231	Gold nanospheres conjugated with AS1411	Nude mice Fox1 <sup>nu</sup> (xenograft)	—	Decreased tumor growth rate and tumor regression (tumor size at 12 days: 100 with nanospheres vs. 1000 mm <sup>3</sup> with control)	1 mg/kg/day (i.p.)	[39]
MDA-MB-231	Hydrogel embedded with gold nanoparticles	SCID hairless congenic mice (orthotopic)	—	Efficient and sustained inhibition of tumor growth (~90% tumor size reduction)	10 nM of gold nanoparticles (i.h.)	[41]
MDA-MB-231	Gold nanomatryoshkas and nanoshells	Sprague-Dawley athymic nude mice (xenograft)	—	Improved survival (83% and 33% at 60 days with nanomatryoshkas and nanoshells respectively) Complete tumor regression at 60 days post-treatment with relapse rates between 16.7% (nanomatryoshkas) and 50% (nanoshells)	300 $\mu$ g of gold (i.v.)	[42]

Table 2. Cont.

Cell Line	NPMBC	Assay	In Vitro		Effect Observed	Doses Assayed	Reference
			Mode of Action/Pathway Involved				
MDA-MB-231	Micellar gold nanoparticles conjugated with ZD6474	Athymic BALB/c (nu+/nu+) mice (xenograft)	—		Decrease in tumor volume (63% of control)	30 mg/kg of ZDD6474 (i.v.)	[44]
BCM-2665A	Gold nanoshells	SCID/beige mice (xenograft)	—		Smaller tumor volume compared to control (400 vs. 800 mm <sup>3</sup> respectively)	~8 × 10 <sup>8</sup> nanoshells/g body weight (i.v.)	[45]
MDA-MB-231	RGD-conjugated mesoporous silica-encapsulated gold nanorods	Nude mice (orthotopic)	—		Smaller tumor volume than control (569 vs. 1302 mm <sup>3</sup> respectively)	~50 µg of gold/g of body weight (i.v.)	[46]
MDA-MB-231	Copper salicylate phenanthroline complexes	Nude mice (xenograft)	—		Smaller tumor volume than control (20 vs. 35 mm <sup>3</sup> respectively)	0.5 mg/mL (i.p.)	[49]
MDA-MB-231	Copper salicylate phenanthroline complexes	Nude mice (xenograft)/Immunohistochemical staining	Ki-67		Reduced Ki-67 expression	0.5 mg/mL (i.p.)	[49]
MDA-MB-231	Water-soluble iminophosphorane ruthenium(II) compounds	NOD.CB17-Prkdc SCID/J mice (xenograft)	—		Significant inhibition of tumor growth and smaller tumor size than control (56% decrease vs. 200% increase in tumor volume respectively)	5 mg/kg/day (i.p.)	[52]
A17	Ruthenium complexes	FVB/NCrl mice (xenograft)	—		Decreased tumor grow rate and smaller tumor size than control (<3 vs. 7 mm)	210 mg/kg/day (i.p.)	[55]
SUM159	Highly crystallized iron oxide nanoparticles	BALB/c immune-competent mice (xenograft)	—		Complete tumor regression without relapses	20 mg iron/kg body weight (i.v.)	[60]
SUM159	Iron oxide nanoparticles	NOD/SCID immune-compromised mice (orthotopic)	—		Smaller tumor size than control	20 mg iron/kg body weight (i.v.)	[61]
4T1	Supermagnetic iron oxide nanoparticles conjugated with doxorubicin	BALB/c mice (orthotopic)	—		Smaller tumor size than control (7 vs. 74 mm <sup>3</sup> respectively)	0.25 mg iron/100 mm <sup>3</sup> (i.t.)	[62]
MDA-MB-231	Chitosan hydrogel cross-linked with telechelic difunctional poly(ethylene glycol) modified iron oxide magnetic nanoparticles	BALB/c mice (xenograft)	—		Smaller tumor size than control (relative tumor volume ~0.75 vs. 4.5 v/v respectively)	18.7 mg/kg (i.t.)	[63]
MDA-MB-231	Silver nanoparticles	nu/nu athymic mice (xenograft)	—		Decreased tumor grow rate and smaller tumor size than control (250 vs. 550 mm <sup>3</sup> respectively)	0.2 µg/mm <sup>3</sup> tumor volume (i.t.)	[66]
MDA-MB-231	Gold nanorod-loaded neural stem cells	Athymic nude mice (xenograft)	—		Complete tumor ablation, improved survival and reduced tumor recurrence compared to control	12.5 µg/(i.t.)	[70]

Abbreviations: —, Not analyzed; Akt, Protein Kinase B; ATM, Ataxia Telangiectasia Mutated Protein; CCK-8, Cell Counting Kit-8; Cdc2, Cell Division Control Protein 2 Homolog; EGFR, Epidermal Growth Factor Receptor; ERK, Extracellular Signal-Regulated Kinase; FAK, Focal Adhesion Kinase; Fox 1, Forkhead Box Protein 1; HSP72, Heat Shock Protein 72; i.h., implantation of a hydrogel disk on top of the tumors; i.p., intraperitoneal injection; i.t., intratumoral injection; i.v., intravenous injection; MRP1, Multidrug Resistance Protein 1; mTOR, Mammalian Target of Rapamycin; MTS, 3-(4,5-Dimethylthiazol-2-yl)-5-(3-Carboxymethoxyphenyl)-2-(4-Sulfonyl)-2H-Tetrazolium; MTT, 3-(4,5-Dimethylthiazol-2-yl)-2,5-Diphenyltetrazolium Bromide; NOD, Non-Obese Diabetic; PI, Propidium Iodide; SCID, Severe Combined Immunodeficient.

**Table 3.** Non-platinum metal based complexes (NPMBC) inhibit the in vitro and in vivo growth of triple-negative breast cancer (TNBC) cells by inducing apoptosis.

In Vitro						
Cell Line	NPMBC	Assay	Mode of Action/Pathway Involved	Effect Observed	Doses Assayed	Reference
MDA-MB-231	Liposome encapsulated ruthenium polypyridine complex	Western blot	PARP Caspase 3 Caspase 8 Caspase 9	Increased cleaved PARP, caspase 3, caspase 8 and caspase 9 levels	5 $\mu$ M	[16]
MDA-MB-231	Liposome encapsulated ruthenium polypyridine complex	Flow cytometry (cell cycle arrest)	—	75.9% apoptotic cells 54% cells in the G2/M phase	5 $\mu$ M	[16]
MDA-MB-231	Gold nanostars	Fluorescent assay qPCR	Caspase 3/7 Bcl-2	Increased caspase activity Downregulation of Bcl-2 expression	0.3 nM	[27]
MDA-MB-231	Multibranched gold nanoantennas	Annexin V/calcein/PI staining assay	—	Induction of apoptotic cell death	170 $\mu$ g/mL	[29]
MDA-MB-231	Gold nanoparticles conjugated gemcitabine	Annexin V/7-AAD assay	—	Induction of apoptosis	0.5, 1, 5, 25 nM	[30]
MDA-MB-231	Anti-EGFR-gold nanorod conjugates	FITC-annexin V/PI staining assay	—	~25–40% apoptotic cells	1.84 $\mu$ g/mL	[37]
MDA-MB-231	Anti-EGFR-gold nanorod conjugates	Western blot	Caspase 3	Increased cleaved caspase 3 protein	1.84 $\mu$ g/mL	[37]
MDA-MB-231	Gold nanospheres	FITC-annexin V/PI staining assay	—	88% apoptotic cells	200 nM	[39]
MDA-MB-231 SUM1315 HCC1937 MDA-MB-468	Gold-nanoparticles conjugated with Rad6 inhibitor	Acridine orange/ethidium bromide staining	—	SUM1315 and MDA-MB-231 cells in early and late stages of apoptosis No morphological alterations consistent with apoptosis were observed in HCC1937 or MDA-MB-468 cells	1–5 $\mu$ M	[40]
SUM1315 HCC1937	Gold-nanoparticles conjugated with Rad6 inhibitor	Mitochondrial membrane potential (JC-1)	—	Loss in the mitochondrial function of SUM1315 cells Mitochondrial function of HCC1937 cells was unaffected	1 $\mu$ M	[40]
SUM1315 HCC1937	Gold-nanoparticles conjugated with Rad6 inhibitor	Western blot	PARP-1	Activation of PARP-1	1–5 $\mu$ M	[40]
MDA-MB-468	Micellar gold nanoparticles conjugated with ZD6474	FITC-annexin V/PI staining assay	—	28.2% apoptotic cells	5 $\mu$ M	[44]
MDA-MB-231	RGD-conjugated mesoporous silica-encapsulated gold nanorods	FITC-annexin V/PI staining assay	—	Increased apoptotic cells	50 $\mu$ g/mL	[46]
MDA-MB-231	RGD-conjugated mesoporous silica-encapsulated gold nanorods	DHE fluorescence method	ROS	Increased cellular ROS levels	50 $\mu$ g/mL	[46]
MDA-MB-231 BT-20	Copper salicylate phenanthroline complexes	Flow cytometry (Annexin V/PI)	—	>80% apoptotic cells	25 $\mu$ M	[49]

Table 3. Cont.

In Vitro						
Cell Line	NPMBC	Assay	Mode of Action/Pathway Involved	Effect Observed	Doses Assayed	Reference
MDA-MB-231 BT-20	Copper salicylate phenanthroline complexes	Western blot	Bcl-2 Bcl-xL Survivin PARP	Decreased Bcl-2, Bcl-xL and surviving expression Increased cleaved PARP expression	25 µM	[49]
MDA-MB-231	Copper oxide nanowire conjugated with folic acid	FITC-annexin V/PI staining assay	—	Induction of apoptosis	2.5 µg/mL	[51]
MDA-MB-231	Copper oxide nanowire conjugated with folic acid	SEM	—	Formation of apoptotic bodies and membrane blebbing	2.5 µg/mL	[51]
MDA-MB-231	Copper oxide nanowire conjugated with folic acid	Flow cytometry	—	Induction of ROS	2.5 µg/mL	[51]
MDA-MB-231	Copper oxide nanowire conjugated with folic acid	Mitochondrial membrane potential (JC-1) Immunofluorescence Western blotting analysis	ROS Cyt C	Loss in the mitochondrial membrane potential Increased expression of Cyt C in the cytosol	2.5 µg/mL	[51]
MDA-MB-231	Copper oxide nanowire conjugated with folic acid	Western blotting analysis	Caspase 3 Caspase 9	Increased cleaved caspase 9 and caspase 3 expression	2.5 µg/mL	[51]
MDA-MB-231	Copper oxide nanowire conjugated with folic acid	Western blotting analysis Immuno-fluorescence staining	NF-κB p65 protein	Inhibition of nuclear transport of the p65 subunit of NF-κB protein	2.5 µg/mL	[51]
MDA-MB-231	Copper oxide nanowire conjugated with folic acid	qRT-PCR Western blot	miR425 PTEN Akt	Down-regulation of miR-425 and Akt, and up-regulation of PTEN	2.5 µg/mL	[51]
MDA-MB-231	Ruthenium-based nucleolipidic nanoaggregates	Phase-contrast microscopy	—	Cell shrinkage and loss of cell-cell contact	14.7 µM	[53]
MDA-MB-231	Ruthenium-based nucleolipidic nanoaggregates	FITC-annexin V/PI staining assay	—	~80% of cells in late apoptosis phase	14.7 µM	[53]
MDA-MB-231	Ruthenium-based nucleolipidic nanoaggregates	DNA fragmentation assay	—	Internucleosomal DNA laddering	14.7 µM	[53]
MDA-MB-231	Ruthenium-based nucleolipidic nanoaggregates	Western blot	Bax Bcl-2 Caspase 3 Caspase 9 Caspase 8	Up-regulated Bax expression Down-regulated Bcl-2 expression Activation of caspase 9, caspase 8 and caspase 3	14.7 µM	[53]
MDA-MB-231 HCC1937	Ruthenium complexes	RT-PCR	P21 p53 BRCA1	Upregulated p53, P21 and BRCA1 expression	13.2 and 14.1 µM for MDA-MB-231; 1.8 and 9.9 µM for HCC1937	[54]
A17 MDA-MB-231	Ruthenium complexes	Immunohistochemistry Western blot	Caspase 3	Increased number of apoptotic cells (cleaved caspase 3 positive cells)	750 µM for A17; 1 mM for MDA-MB-231	[55]

Table 3. Cont.

In Vitro						
Cell Line	NPMBC	Assay	Mode of Action/Pathway Involved	Effect Observed	Doses Assayed	Reference
MDA-MB-231	Ruthenium complexes	DAPI staining	—	Nuclear chromatin condensation with formation of apoptotic bodies	2, 4 and 8 $\mu$ M	[58]
MDA-MB-231	Ruthenium complexes	Flow cytometry (PE annexin-V)	—	43% apoptotic cells	2 $\mu$ M	[58]
MDA-MB-231	Ruthenium complexes	qRT-PCR	Bax Caspase 3 Bcl-2	Increased Bax and caspase 3 expression Decreased Bcl-2 expression	4, 8 and 16 $\mu$ M	[58]
MDA-MB-231	Ruthenium complexes	Western blotting	Bax Caspase 3 Bcl-2	Increased Bax expression Decreased Bcl-2 expression No change in caspase-3 expression	0.5, 1, 2, 4, 8 and 16 $\mu$ M	[58]
MDA-MB-231	Ruthenium complexes	Comet assay	—	DNA damage	4 and 8 $\mu$ M	[58]
MDA-MB-231	Ruthenium-based compounds	DAPI staining	—	Nuclear fragmentation	60 and 70 $\mu$ M	[59]
MDA-MB-231	Ruthenium-based compounds	Flow cytometry (PE annexin-V)	—	74.4% apoptotic cells	20 $\mu$ M	[59]
MDA-MB-231	Ruthenium-based compounds	qRT-PCR	Bax Caspase 3 Bcl-2	Increased expression of Bax and caspase 3. No change in gene expression of Bcl-2	40 $\mu$ M	[59]
MDA-MB-231	Ruthenium-based compounds	Western blotting	Caspases 3 and 9	Increased caspase 3 and 9 expression	2.5 $\mu$ M	[59]
MDA-MB-231	Ruthenium-based compounds	Western blotting	Bcl-2	No change in Bcl-2 expression	10 $\mu$ M	[59]
MDA-MB-231	Supermagnetic iron oxide nanoparticles conjugated with doxorubicin	Mitochondrial membrane potential (JC-1)	—	Increased depolarization of mitochondrial membrane potential	520 $\mu$ M	[62]
MDA-MB-231 HCC 1806	Iron oxide nanoparticles linked antagonist for leptin	Immunoblotting analysis	STAT3	Prevention of leptin-induced STAT3 expression only in HCC1806 cells	0.0036 pmol/L	[64]
MDA-MB-231	Doxorubicin-hyaluronan conjugated iron oxide nanoparticles	FITC-annexin V/PI staining assay	—	12% apoptotic cells (early and late stages of apoptosis)	2 $\mu$ M	[65]
MDA-MB-231	Doxorubicin-hyaluronan conjugated iron oxide nanoparticles	Steady-Glo luciferase reagent assay	NF- $\kappa$ B	Reduced NF- $\kappa$ B transcriptional activity (~40%)	2 $\mu$ M	[65]
MDA-MB-231	Silver nanoparticles	FITC-annexin V/PI staining assay	—	Cells in early and late stages of apoptosis	1.25–10 $\mu$ g/mL	[67]
MDA-MB-231	Silver nanoparticles	Comet assay	—	DNA damage	5 and 10 $\mu$ g/mL	[67]
MDA-MB-231	Silver nanoparticles	Flow cytometry Confocal microscopy Fluorescence microscopy	ROS	Increase ROS levels	2.5, 5 and 10 $\mu$ g/mL	[67]

Table 3. Cont.

In Vitro						
Cell Line	NPMBC	Assay	Mode of Action/Pathway Involved	Effect Observed	Doses Assayed	Reference
MDA-MB-231	Rhodium(III) complex	Western blot	Caspase 3 Caspase 7 Caspase 8 Bcl-2 PARP	Increased PARP, and cleaved caspases-3, -7, and -8 expression Decreased Bcl-2 expression	1 and 3 $\mu$ M	[69]
In Vivo						
Cell Line	NPMBC	Animal (Model)/Analysis from Animal Tissue	Mode of Action/Pathway Involved	Effect Observed	Doses Assayed (Route of Administration)	Reference
MDA-MB-231	Liposome encapsulated ruthenium polypyridine complex	Athymic nude mice (orthotopic)/Western blot, immunohistochemistry	PARP Caspase 3 Caspase 8 Caspase 9 TUNEL	Increased TUNEL cleaved PARP, caspase 3, caspase 8 and caspase 9 levels	5 mg ruthenium/kg (i.v.)	[16]
MDA-MB-231	CD44-targeting HSP72 depletion nanosystem based on plasmonic gold nanoparticles	Immunohistochemistry	TUNEL	Massive apoptotic cells	10 mg/kg (i.v.)	[28]
MDA-MB-231	Anti-EGFR-gold nanorod conjugates	BALB/c nude mice (xenograft)/ Immunohistochemistry	TUNEL Caspase 3	Increased TUNEL and caspase 3 levels	0.5 pmol/g mouse (i.v.)	[37]
MDA-MB-231	Copper salicylate phenanthroline complexes	Nude mice (xenograft)/ Immunohistochemical staining	Bcl-2 Bcl-xL Survivin	Reduced Bcl-2, survivin and Bcl-xL expression	0.5 mg/mL (i.p.)	[49]
4T1	Copper oxide nanowire conjugated with folic acid	Immunohistochemical analysis of tumors of BALB/c mice (orthotopic)	—	Suppression of tumor growth (lower tumor weight and volume)	2.5 mg/kg body weight (i.p.)	[51]
4T1	Copper oxide nanowire conjugated with folic acid	Immunohistochemical analysis of tumors of BALB/c mice (orthotopic)/Immunohistochemical analysis and western blot	PTEN miR425	Increased PTEN expression and decreased miR-425 expression	2.5 mg/kg body weight (i.p.)	[51]
A17	Ruthenium complexes	FVB/NCr1 mice (xenograft)/Immunohistochemistry analysis	Caspase 3	Increased number of apoptotic cells in tumors (cleaved caspase-3 positive cells)	210 mg/kg/day (i.p.)	[55]

Abbreviations: —, Not analyzed; 7-AAD, 7-Aminoactinomycin D; Akt, Protein Kinase B; Bax, Bcl-2-Like Protein 4; Bcl-2, B-Cell Lymphoma 2; Bcl-XL, B-Cell Lymphoma-Extra Large; BRCA1, Breast Cancer Susceptibility Gene 1; Cyt C, Cytochrome C; DAPI, 4',6-Diamidino-2-Phenylindole; DHE, Dihydroethidium; EGFR, Epidermal Growth Factor Receptor; FITC, Fluorescein Isothiocyanate; HSP72, Heat Shock Protein 72; i.p., intraperitoneal injection; i.v., intravenous injection; miR425, microRNA425; NF- $\kappa$ B, Nuclear Factor Kappa-Light-Chain-Enhancer of Activated B Cells; p65 protein, Nuclear factor NF- $\kappa$ B P65 Subunit; PARP, Poly(ADP-ribose) POLYMERASE; PE, Phycocerythrin; PI, Propidium Iodide; PTEN, Phosphatase and Tensin Homolog; qRT-PCR, Quantitative Reverse Transcription Polymerase Chain Reaction; ROS, Reactive Oxygen Species; SEM, Scanning Electron Microscopy; STAT3, Signal Transducer and Activator of Transcription 3; TUNEL, Terminal Deoxynucleotidyl Transferase dUTP Nick End Labeling.

**Table 4.** Non-platinum metal based complexes (NPMBC) inhibit the in vitro and in vivo growth of triple-negative breast cancer (TNBC) cells by inducing autophagic cell death.

In Vitro						
Cell Line	NPMBC	Assay	Mode of Action/Pathway Involved	Effect Observed	Doses Assayed	Reference
MDA-MB-231	Anti-EGFR-gold nanorod conjugates	Immunofluorescence staining	LC3	Increased LC3 expression	120 pM	[38]
MDA-MB-231	Anti-EGFR-gold nanorod conjugates	TEM	—	Induction of double- or multiple-membrane vesicles	120 pM	[38]
MDA-MB-231	Anti-EGFR-gold nanorod conjugates	Western blot	Beclin-1 Atg5 p62 LC3 Akt mTOR	Increased Beclin-1, Atg5, LC3-II, and p62 expression Decreased phosphorylation of mTOR and Akt	120 pM	[38]
MDA-MB-231 SUM1315	Gold-nanoparticles conjugated with Rad6 inhibitor	Western blot	LC3-I LC3-II p62	Increased conversion of LC3-I to LC3-II in SUM1315 cells Decreased p62 expression in SUM1315 cells No changes in LC3-I/II ratios or expression of p62 protein in MDA-MB-231 cells	1–5 $\mu$ M	[40]
MDA-MB-231	Ruthenium-based nucleolipidic nanoaggregates	Phase-contrast microscopy Monodansylcadaverine assay	—	Increased formation of autophagic vacuoles	12.1–14.7 $\mu$ M	[53]
In Vivo						
Cell Line	NPMBC	Animal (Model)/Analysis from Animal Tissue	Mode of Action/Pathway Involved	Effect Observed	Doses Assayed (Route of Administration)	Reference
MDA-MB-231	Anti-EGFR-gold nanorod conjugates	BALB/c nude mice (xenograft)	—	Significant decrease in tumor volume compared to control (120 vs. 250 mm <sup>3</sup> )	0.5 pmol/g mouse (i.v.)	[38]
MDA-MB-231	Anti-EGFR-gold nanorod conjugates	BALB/c nude mice (xenograft)/Histological analysis	Beclin-1 LC3	Enhanced beclin-1 and LC3 expression	0.5 pmol/g mouse (i.v.)	[38]

Abbreviations: —, Not analyzed; Akt, Protein Kinase B; Atg5, Autophagy Related 5 Protein; EGFR, Epidermal Growth Factor Receptor; i.v., intravenous injection; LC3, Microtubule-Associated Protein 1A/1B-Light Chain 3; mTOR, Mammalian Target of Rapamycin; p62, Nucleoporin p62; TEM, Transmission Electron Microscopy.

**Table 5.** Non-platinum metal based complexes (NPMBC) inhibit the in vitro and in vivo growth of triple-negative breast cancer (TNBC) cells by inhibiting migration, invasion and/or metastasis.

In Vitro						
Cell Line	NPMBC	Assay	Mode of Action/Pathway Involved	Effect Observed	Doses Assayed	Reference
MDA-MB-231	Chitosan layered gold nanorods	Transwell assay	—	Inhibition of cell migration	50 nM	[43]
MDA-MB-231	Micellar gold nanoparticles conjugated with ZD6474	Boyden chamber assay	—	~90% inhibition of cell invasion and migration	1 $\mu$ M	[44]
MDA-MB-231	Copper oxide nanowire conjugated with folic acid	Wound healing assay	—	85% inhibition of cell migration	1.25 $\mu$ g/mL	[51]
MDA-MB-231	Copper oxide nanowire conjugated with folic acid	Transwell migration assay	—	80% inhibition of cell migration	1.25 $\mu$ g/mL	[51]
MDA-MB-231	Copper oxide nanowire conjugated with folic acid	Immunocytochemistry	FAK PTEN	Decreased FAK expression Up-regulated PTEN expression	1.25 $\mu$ g/mL	[51]
MDA-MB-231	Ruthenium-based complexes	Transwell assay	—	90.8% inhibition of cell invasion	4 $\mu$ M	[58]
MDA-MB-231	Ruthenium-based complexes	Wound healing assay	—	79% inhibition of cell migration	4 $\mu$ M	[58]
MDA-MB-231	Ruthenium-based complexes	Adhesion assay	Type I collagen Fibronectin Laminin Vitronectin	35–70% inhibition of cancer cell adhesion to extracellular matrix proteins	8 $\mu$	[58]
MDA-MB-231	Ruthenium-based complexes	Wound healing assay	—	Inhibition of cell migration	5, 10 and 20 $\mu$ M	[59]
MDA-MB-231	Ruthenium-based complexes	Transwell assay	—	80% inhibition of cell invasion	20 $\mu$ M	[59]
MDA-MB-231	Ruthenium-based complexes	Zymography assay	MMP-9	60% of inhibition of MMP-9 expression	20 $\mu$ M	[59]
MDA-MB-231	Ruthenium-based complexes	Adhesion assay	Type I collagen Fibronectin Laminin Vitronectin	50–65% inhibition of cancer cell adhesion to type I collagen, fibronectin, laminin, vitronectin	40 $\mu$ M	[59]
MDA-MB-231 4T1	Supermagnetic iron oxide nanoparticles conjugated with doxorubicin	Wound healing assay	—	Minimal closure of the scratch	520 $\mu$ M	[62]
MDA-MB-231	Doxorubicin-hyaluronan conjugated iron oxide nanoparticles	Confocal microscopy	Vimentin e-cadherin	Decreased vimentin expression No change in e-cadherin expression	2 $\mu$ M	[65]
MDA-MB-231	Doxorubicin-hyaluronan conjugated iron oxide nanoparticles	ELISA	IL-6 IL-10	Decreased IL-6 secretion No change in secretion of IL-10	2 $\mu$ M	[65]

Table 5. Cont.

In Vitro						
Cell Line	NPMBC	Assay	Mode of Action/Pathway Involved	Effect Observed	Doses Assayed	Reference
MDA-MB-231	Doxorubicin-hyaluronan conjugated iron oxide nanoparticles	Steady-Glo luciferase reagent assay	NF- $\kappa$ B	Reduced NF- $\kappa$ B transcriptional activity (~40%)	2 $\mu$ M	[65]
In Vivo						
Cell Line	NPMBC	Animal (Model)/Analysis from Animal Tissue	Mode of Action/Pathway Involved	Effect Observed	Doses Assayed (Route of Administration)	Reference
T41	Iron oxide nanoparticles	BALB/c immune-competent mice (xenograft)	—	Lower lung metastatic nodules than control (13 vs. 42)	20 mg iron/kg body weight (i.v.)	[61]
SUM159	Iron oxide nanoparticles	NOD/SCID immune-compromised mice (orthotopic)	—	Lower incidence of lymph node metastasis than control (25% vs. 62.5%)	20 mg iron/kg body weight (i.v.)	[61]
4T1	Supermagnetic iron oxide nanoparticles conjugated with doxorubicin	BALB/c mice (orthotopic)	$\alpha$ v $\beta$ 3	Lower metastatic colonies than control (~<1 vs. ~10 at lung respectively; ~1 vs. ~3 at liver respectively) which could be related with the inhibition of $\alpha$ v $\beta$ 3	0.25 mg iron/100 mm <sup>3</sup> (i.t.)	[62]

Abbreviations: —, Not analyzed; ELISA, Enzyme-Linked ImmunoSorbent Assay; FAK, Focal Adhesion Kinase; IL, Interleukin; i.t., intratumoral injection; i.v., intravenous injection; MMP, Matrix Metalloproteinases; NF- $\kappa$ B, Nuclear Factor Kappa-Light-Chain-Enhancer of Activated B Cells; PKM, Pyruvate Kinase Isozymes; PTEN, Phosphatase and Tensin Homolog.

Cellular studies constitute an important step in the development of drugs; however, demonstrating efficacy in suitable animal models and validating cellular observations *in vivo* are a condition *sine qua non* for clinical trials investigating potential anticancer agents. Inconsistencies in results between *in vitro* and *in vivo* systems concerning the anticancer effect of NPMBC can be related to differences in their pharmacokinetic behavior, thus their study is necessary. In this way, NPMBC seem to have good *in vivo* pharmacokinetic properties. They are absorbed quickly into plasma [16,39,44,52], the circulation time in the bloodstream is long [42], their uptake in the tumor tissue is significant [16,28,32,37,39,41,42,44,46,51,52,60,70], their accumulation in organs (brain, liver, kidney, spleen, heart, lung, and intestine) is low [16,28,39,41,42,44,51,52,55] and the clearing rate is good [51].

A large proportion of current knowledge about the therapeutic potential of NPMBC is derived from *in vitro* and *in vivo* studies performed using TNBC cell lines. TNBC MDA-MB-231 cell models are considered the most reliable models of TNBC [71,72], so this cell line is the world's most commonly used human TNBC cell line. However, this raises the issue on how representative this cell line is of the broad spectrum of TNBCs (Table 1).

### 2.1. Suppression of Cancer Cell Viability in Association with the Induction of Cell Death

NPMBC-mediated inhibition of breast carcinogenesis is associated with reduced cellular proliferation (Table 2) together with the induction of programmed cell death (Tables 3 and 4). Apoptosis is by far the primary mode of programmed cell death (Table 3), but sometimes it is coupled to the induction of autophagy, as can be suspected from the few studies which have been carried out (Table 4).

NPMBC display good cytotoxic behavior *in vitro* and are able to reduce the growth of primary tumors (Table 2). NPMBC inhibit the growth of TNBC cells better than non-TNBC cells [66]. Furthermore, NPMBC of which effects are dose- [49,53,55,67] and time- [63,67] dependent could be more cytotoxic than platinum-based drugs [52,53,57,58,68]. For example, Biancalana et al. [57] observed that ruthenium complexes have good cytotoxic activity, with  $IC_{50}$  values substantially lower than the values obtained with cisplatin on MDA-MB-231 cells. These differences could be due to the fact that they have different mechanisms of action; for example, the activation of p53-dependent or p53-independent checkpoints by cisplatin or ruthenium complexes, respectively [9,52,54,68]. Since platinum-based drugs and NPMBC act on different pathways, NPMBC could be a new therapeutic option for patients with TNBC resistant to platinum-based drugs.

Avoiding apoptosis is a hallmark of cancer and an important mechanism in resistance to therapies. Apoptosis is preferred over necrosis because the latter elicits inflammation and undesirable immunogenic responses [73]. NPMBC induce significant apoptotic activity in TNBC cells which can be mediated by multiple mechanisms (Table 3). When MDA-MB-231 and BT-20 cells were treated with 25  $\mu$ M copper salicylate phenanthroline complexes, more than 80% of TNBC cells underwent apoptosis through down-regulation of the anti-apoptosis proteins Bcl-2, Bcl-xL and survivin and up-regulation of cleaved PARP [49]. These findings confirm the participation of protease enzyme caspases in the programmed cell death induced by NPMBC. However, NPMBC can also activate caspase-independent pathways acting on mitochondria. For example, when MDA-MB-231 cells were treated with 10  $\mu$ g/mL of silver nanoparticles, high intracellular levels of reactive oxygen species (ROS) were observed at 24 h of incubation [67]. These free radicals destabilize the mitochondria and induce apoptosis [74] acting on Bcl-2 family proteins [75]. Considering that TNBC is more susceptible to drugs that cause oxidative stress than other BC types [66], these compounds could be a hopeful alternative method for its treatment. Besides what was mentioned above, we must not forget that the efficacy of several NPMBC relies on their capacity to influence the tumor–host interaction and modify the immune microenvironment, inducing a form of apoptosis in cancer cells known as “immunogenic cell death”. Thus, Montani et al. [55] observed that ruthenium complexes reverse tumor-associated immune suppression leading to the activation of an immune response specific for TNBC cells.

The NPMBC can be synthesized by chemical [76], physical [77] and biological methods [35], all with cytotoxic activity against TNBC cells. Although chemical and physical syntheses have been

the most widely used strategies, there is growing interest in the biosynthesis of NPMBC because of its numerous advantages (for example, economical, safe, and inert) [78,79].

The NPMBC differ in shape [34], size [31–33,42], dose [30,36,66], synthesis procedure (see previous paragraph), composition [50,56], capping agent [33,80], particle surface charges [31] and structure [56,68,69]. All of these features can affect their cellular uptake and therefore also their cytotoxic activity. In general, modified small nanoparticles with low surface charges ( $-15$  mV) have better cellular internalization than large nanoparticles, however both extremely small ( $<25$  nm) and large ( $>80$  nm) nanoparticles displayed a low cellular uptake [31,33]. On the other hand, it has been demonstrated that replacing ruthenium with iron gives compounds with high antiproliferative activity ( $IC_{50} = 0.09$  vs.  $>30$   $\mu$ M), the compounds with the shortest carbon chain linking the two cyclopentadienyl rings being the most active [56]. Finally, another interesting finding is the superiority of nanorods over nanospheres for photothermal cancer therapy (PCT) using gold nanoparticles [34]. Despite this evidence, it has not been possible to establish a linear correlation between cellular responses and the characteristics of NPMBC because there is wide interstudy variability (for example, in relation to cell lines, measurement methods, etc.).

NPMBC possess cytotoxic activity per se [39,66,67,69]; however, their main applications are related to their ability to act as radiosensitizers in cancer cells through the induction of G2/M phase cell cycle arrest [36,47,66], as agents for PCT applications [14,28,29,37,63] or as transmembrane carriers for the controlled release and targeted delivery of anticancer drugs increasing their cellular uptake [30,39,40], among others [47,64]. Cancer cells in a tumor are very heterogeneous, that is, they differ in marker expression, morphology, proliferation capacity, growth stage, etc. This heterogeneity increases the need for combining therapeutic agents with different action mechanisms. Although few studies have examined the role of NPMBC for combination chemotherapy, recently the utility of iron oxide magnetic nanoparticles as multidrug codelivery system for synergistic chemotherapy has been demonstrated [63].

The effects of NPMBC on TNBC cells, as well as on cancer cells from other solid tumors, is facilitated by abnormalities of the tumor vasculature, such as hypervascularization, high production of vascular permeability factors, etc. [81]. However, intrinsic properties of NPMBC are not less important. For example, nanoparticles are characterized by their high permeability [82] and retention effect [83] which results in potentiation of the cytotoxic effects with minimal side effects [39,49]. When the tyrosine kinase inhibitor ZD6474 was conjugated with gold nanoparticles, besides inducing a higher antiproliferative effect than the ZD6474 alone under in vitro conditions, it also reduced the size of tumors induced in mice more efficiently than the drug alone [44]. These properties could be useful to counteract drug resistance mechanisms, the main limitation to the success of conventional therapy. In this sense, Conde et al. [41] showed that gold nanoparticles loaded with 5-fluorouracil ( $IC_{50} = \sim 0.5$  nM) decrease the viability of 5-fluorouracil-resistant MDA-MB-231 cells by silencing the cell surface efflux pump MRP1.

One of the concerns for developing NPMBC as therapeutic agents for TNBC treatment could be their toxicity. However, several studies have proven their harmlessness in normal cells [39,49,52,57,66,84]. Ruthenium(II) paracyme complexes showed a moderate selectivity for TNBC cells, so normal cells (human skin fibroblasts) were less affected than MDA-MB-231 cells [57]. Likewise, when copper salicylate phenanthroline complexes [49], ruthenium complexes [55] or gold nanoparticles [28,37,39] were administered to mice, they were well tolerated as evidenced by the lack of weight loss, behavior of the animal or examination of organs.

It is hypothesized that, because of their capacity for self-renewal, differentiation and apoptosis-resistance [85], cancer stem cells (CSCs, also referred to as tumor-initiating cells) could be responsible for the cancer formation [61]. What is more, they could be resistant to conventional treatments and contribute to the recurrence after treatment [86]. Gold nanoshells seem to sensitize breast CSCs to radiation therapy mediated by the activation of the heat shock proteins (HSP) HSP40, HSP60, HSP70 and HSP90 $\alpha$  [45]. Likewise, CSCs' ability to self-renew might be inhibited by iron

oxide nanoparticle-mediated PCT [61] or iron oxide nanoparticles-linked leptin antagonist [64] which has been demonstrated through the reduction of mammospheres/tumorspheres of MDA-MB-231 and SUM 159 cells [61,64]. Although these findings are hopeful, new strategies for improving the intratumoral distribution of NPMBC are necessary to achieve a homogeneous nanoparticle distribution within the tumor without depositing them in surrounding healthy tissue [70].

## 2.2. Migration, Invasion and/or Metastasis

Metastasis is a cascade of events where tumor cells disseminate from the primary tumor to distant sites, with the migration of tumor cells being a prerequisite for tumor-cell invasion and metastasis (Figure 1) [87]. Thus, any factor which regulates this process might be a target for anti-metastatic therapeutic strategies (Table 5). The poor prognosis of the triple negative subtype reflects the aggressive biology of this disease and the difficulty of its treatment, especially when it metastasizes.

Study of the anti-metastatic effect of NPMBC on TNBC cells is very recent. It has been shown that NPMBC, besides enhancing the potential of anticancer therapies [43,44,62], can be used as monotherapy [43,51] to prevent cancer cell migration, invasion and/or metastasis. These findings were confirmed by Paholak et al. [61] using in vivo models. When immunocompromised NOD/SCID mice were inoculated with TNBC cells, it was observed that those mice that received nanoparticle-mediated PCT prior to surgical tumor resection had lower incidence of metastasis to the lung than those which had been treated only with surgery. If these findings were observed in humans, combination therapy consisting of nanoparticle-mediated PCT and surgery would provide a treatment option for patients with metastatic breast cancer, a disease which nowadays has no cure [88].

Unfortunately, little is known about the mechanisms underlying the anti-metastatic effect of NPMBC (Figure 1 and Table 5). However, available evidence suggests that their action could be mediated by the inhibition of matrix metalloproteinases (MMPs) [59], enzymes with the ability to degrade extracellular matrix proteins, after interaction with the  $\alpha v\beta 3$  integrin receptor [62]. Likewise, it has been suggested that NPMBC could inhibit epithelial–mesenchymal transition [65] and modify the structure of the actin cytoskeleton, interfering with the function of integrins [58,59] and under-regulating the phosphorylation of the focal adhesion kinase (FAK) [51]. No less important are the studies which highlight their role in inflammation [89,90]. On the one hand, it has been observed that doxorubicin-hyaluronan conjugated iron oxide nanoparticles reduce the secretion of the pro-inflammatory IL-6, an important prognostic indicator in patients with TNBC [91], and which is thought to contribute to their invasiveness [92]; on the other hand, it has been suggested that iron oxide nanoparticle-mediated hyperthermia could trigger the release of inflammatory mediators which would induce a systemic cancer-specific immune response in which cytotoxic T-cells would recognize and inhibit distal cancer cells [89].

One of the major limitations of anti-metastatic chemotherapy, as has already been mentioned for the treatment of primary tumors, is the toxicity which underlies the importance of targeted therapies. Anticancer drugs should be delivered and act only at the site of action. In this respect, nanoparticles are worthy of mention because they more effectively inhibit the migration of TNBC cells compared to non-tumor cells [51]. Sarkar et al. [44] found potentiation of the anti-migration and anti-invasion effect of the tyrosine kinase inhibitor ZD6474 when it was conjugated to gold nanoparticles synthesized in micellar networks of an amphiphilic block copolymer. On the other hand, the conjugation of interfering RNA (siRNA) to nanoparticles in order to suppress the expression of proteins is another interesting approach. It has been shown that chitosan-layered gold nanorods can be used for silencing genes related to the invasion of TNBC cells [43]. Another strategy which enables the selectivity for tumor cells to be enhanced is by attaching nanoparticles to ligands that bind to receptors expressed on the surface of cancer cells, as has been highlighted by Ahir et al. [51]. Considering that folate receptor expression is elevated in BC cells [93], this receptor could be a good target for cancer treatment. Copper oxide nanowires conjugated with folic acid prevent the motility of MDA-MB-231 cells, an effect that has been validated in vivo [51].

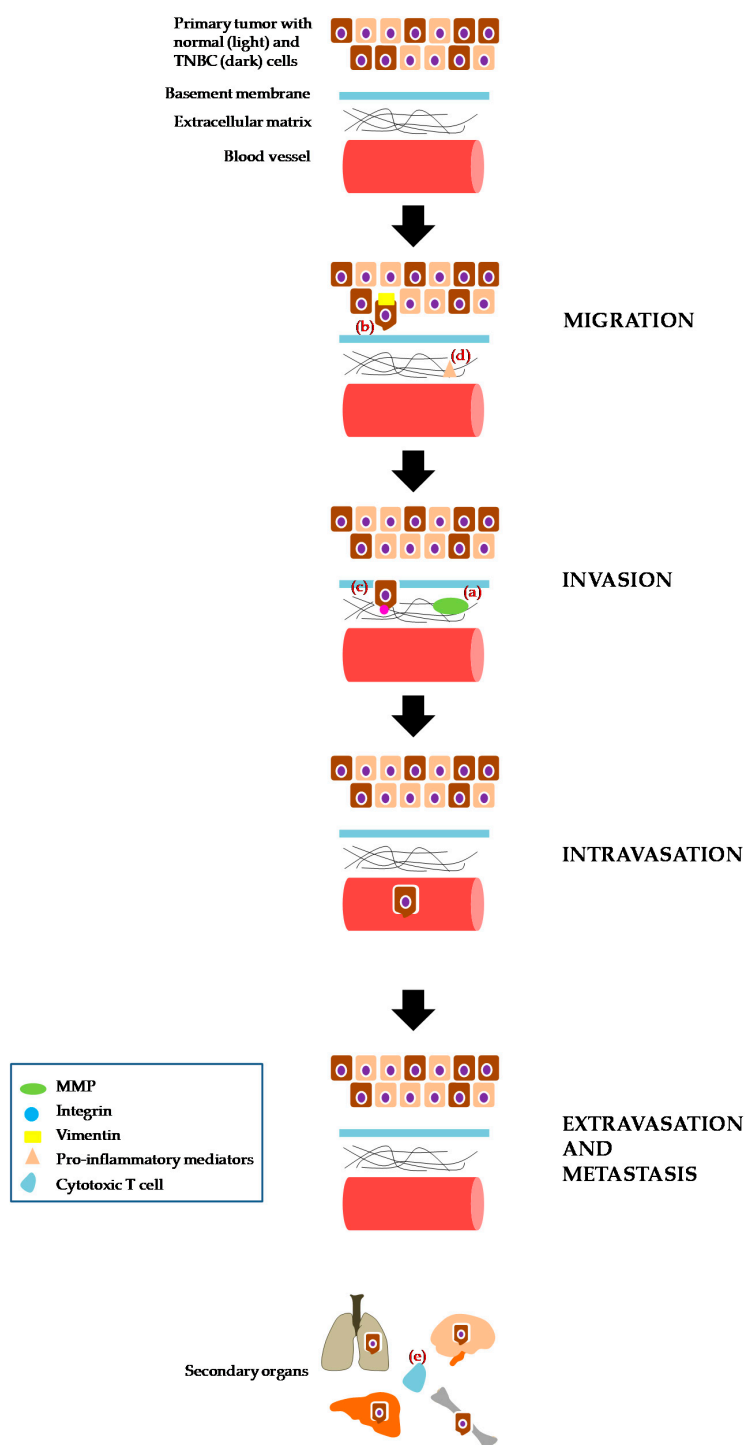


**Figure 1.** Schematic representation of the metastatic process in triple negative breast cancer (TNBC) and its inhibition by non-platinum metal-based complexes (NPMBC). Metastasis is a sequential and interrelated multi-step process that consists of four main essential steps: migration to adjacent tissue after detachment from a primary tumor; local invasion of cancer cells into adjacent tissue; trans-endothelial migration of cancer cells into vessels (intravasation); transport of cancer cells through the circulatory system with extravasation of them in a secondary organ (brain, lung, liver, bone). The anti-metastatic effect of NPMBC has been associated with their ability: to inhibit matrix metalloproteinases (a); to inhibit mesenchymal markers such as vimentin (b); to interfere with the function of integrins (c); and to modify the immune/inflammatory response (d,e).

### 3. Conclusions

Anticancer drugs with new molecular mechanisms of action are necessary for chemotherapy treatment of TNBC, with NPMBC emerging as an upcoming treatment modality. It has been suggested that NPMBC could have an effect on different TNBC cell lines, both in vitro and in vivo. In this way, it has been shown that NPMBC are responsible for activating programmed cell death and exhibiting activity against metastasis. Despite these findings, more studies with different cell lines are required to explore other pathways which could contribute to the control of the broad spectrum of TNBC.

**Author Contributions:** E.M.D.M. contributed substantially to the conception of the work, analysis of data, drafting, critical revision and supervision of the submitted manuscript. D.G.M.-M. contributed substantially to the conception of the work, analysis of data, drafting and critical revision of the submitted manuscript. L.V.-G. and D.L.-A. contributed substantially to the design of the work, acquisition and analysis of data, and drafting of the submitted manuscript. M.J.N.-I. contributed substantially to the design of the work, acquisition, analysis and interpretation of data, and drafting of the submitted manuscript. M.F.-G. contributed substantially to the conception of the work, interpretation of data and critical revision of the submitted manuscript. S.N. contributed substantially to the analysis and interpretation of data, design, drafting, critical revision and supervision of the submitted manuscript. Furthermore, all authors have approved the final version to be published and are accountable for all aspects of the work in ensuring that questions related to the accuracy or integrity of any part of the work are appropriately investigated, resolved and documented in the literature.

**Funding:** This research received no external funding.

**Conflicts of Interest:** The authors declare no conflict of interest.

### References

1. World Health Organization. Breast Cancer. Available online: <http://www.who.int/cancer/prevention/diagnosis-screening/breast-cancer/en/> (accessed on 27 July 2018).
2. Howell, A.; Anderson, A.S.; Clarke, R.B.; Duffy, S.W.; Evans, D.G.; Garcia-Closas, M.; Gescher, A.J.; Key, T.J.; Saxton, J.M.; Harvie, M.N. Risk Determination and Prevention of Breast Cancer. *Breast Cancer Res.* **2014**, *16*, 446. [[CrossRef](#)] [[PubMed](#)]
3. Ricks-Santi, L.; McDonald, J.T.; Gold, B.; Dean, M.; Thompson, N.; Abbas, M.; Wilson, B.; Kanaan, Y.; Naab, T.J.; Dunston, G. Next Generation Sequencing Reveals High Prevalence of BRCA1 and BRCA2 Variants of Unknown Significance in Early-Onset Breast Cancer in African American Women. *Ethn. Dis.* **2017**, *27*, 169–178. [[CrossRef](#)] [[PubMed](#)]
4. Dai, X.; Cheng, H.; Bai, Z.; Li, J. Breast Cancer Cell Line Classification and Its Relevance with Breast Tumor Subtyping. *J. Cancer* **2017**, *8*, 3131–3141. [[CrossRef](#)] [[PubMed](#)]
5. Zaha, D.C. Significance of Immunohistochemistry in Breast Cancer. *World J. Clin. Oncol.* **2014**, *5*, 382–392. [[CrossRef](#)] [[PubMed](#)]
6. Aysola, K.; Desai, A.; Welch, C.; Xu, J.; Qin, Y.; Reddy, V.; Matthews, R.; Owens, C.; Okoli, J.; Beech, D.J.; et al. Triple Negative Breast Cancer—An Overview. *Hered. Genet.* **2013**, *2013*. [[CrossRef](#)]
7. Sharma, P. Update on the Treatment of Early-Stage Triple-Negative Breast Cancer. *Curr. Treat. Options Oncol.* **2018**, *19*, 22. [[CrossRef](#)] [[PubMed](#)]
8. Miller, E.; Lee, H.J.; Lulla, A.; Hernandez, L.; Gokare, P.; Lim, B. Current Treatment of Early Breast Cancer: Adjuvant and Neoadjuvant Therapy. *F1000Res* **2014**, *3*, 198. [[CrossRef](#)] [[PubMed](#)]
9. Hongthong, K.; Ratanaphan, A. BRCA1-Associated Triple-Negative Breast Cancer and Potential Treatment for Ruthenium-Based Compounds. *Curr. Cancer Drug Targets* **2016**, *16*, 606–617. [[CrossRef](#)] [[PubMed](#)]
10. Chavez, K.J.; Garimella, S.V.; Lipkowitz, S. Triple Negative Breast Cancer Cell Lines: One Tool in the Search for Better Treatment of Triple Negative Breast Cancer. *Breast Dis.* **2010**, *32*, 35–48. [[CrossRef](#)] [[PubMed](#)]
11. Lehmann, B.D.; Bauer, J.A.; Chen, X.; Sanders, M.E.; Chakravarthy, A.B.; Shyr, Y.; Pietenpol, J.A. Identification of Human Triple-Negative Breast Cancer Subtypes and Preclinical Models for Selection of Targeted Therapies. *J. Clin. Investig.* **2011**, *121*, 2750–2767. [[CrossRef](#)] [[PubMed](#)]
12. Neve, R.M.; Chin, K.; Fridlyand, J.; Yeh, J.; Baehner, F.L.; Fevr, T.; Clark, L.; Bayani, N.; Coppe, J.P.; Tong, F.; et al. A Collection of Breast Cancer Cell Lines for the Study of Functionally Distinct Cancer Subtypes. *Cancer Cell* **2006**, *10*, 515–527. [[CrossRef](#)] [[PubMed](#)]

13. Jiang, G.; Zhang, S.; Yazdanparast, A.; Li, M.; Pawar, A.V.; Liu, Y.; Inavolu, S.M.; Cheng, L. Comprehensive Comparison of Molecular Portraits Between Cell Lines and Tumors in Breast Cancer. *BMC Genomics* **2016**, *17*, 525. [[CrossRef](#)] [[PubMed](#)]
14. Webb, J.A.; Ou, Y.C.; Faley, S.; Paul, E.P.; Hittinger, J.P.; Cutright, C.C.; Lin, E.C.; Bellan, L.M.; Bardhan, R. Theranostic Gold Nanoantennas for Simultaneous Multiplexed Raman Imaging of Immunomarkers and Photothermal Therapy. *ACS Omega* **2017**, *2*, 3583–3594. [[CrossRef](#)] [[PubMed](#)]
15. Tao, Y.; Li, M.; Auguste, D.T. Pattern-Based Sensing of Triple Negative Breast Cancer Cells with Dual-Ligand Cofunctionalized Gold Nanoclusters. *Biomaterials* **2017**, *116*, 21–33. [[CrossRef](#)] [[PubMed](#)]
16. Shen, J.; Kim, H.C.; Wolfram, J.; Mu, C.; Zhang, W.; Liu, H.; Xie, Y.; Mai, J.; Zhang, H.; Li, Z.; et al. A Liposome Encapsulated Ruthenium Polypyridine Complex as a Theranostic Platform for Triple-Negative Breast Cancer. *Nano Lett.* **2017**, *17*, 2913–2920. [[CrossRef](#)] [[PubMed](#)]
17. Zhao, Y.; Pang, B.; Luehmann, H.; Detering, L.; Yang, X.; Sultan, D.; Harpstrite, S.; Sharma, V.; Cutler, C.S.; Xia, Y.; et al. Gold Nanoparticles Doped with (199) Au Atoms and Their Use for Targeted Cancer Imaging by SPECT. *Adv. Healthc. Mater.* **2016**, *5*, 928–935. [[CrossRef](#)] [[PubMed](#)]
18. Zhang, M.; Kim, H.S.; Jin, T.; Yi, A.; Moon, W.K. Ultrasound-Guided Photoacoustic Imaging for the Selective Detection of EGFR-Expressing Breast Cancer and Lymph Node Metastases. *Biomed. Opt. Express* **2016**, *7*, 1920–1931. [[CrossRef](#)] [[PubMed](#)]
19. Abulrob, A.; Corluka, S.; Blasiak, B.; Gino Fallone, B.; Ponjevic, D.; Matyas, J.; Tomanek, B. LyP-1 Conjugated Nanoparticles for Magnetic Resonance Imaging of Triple Negative Breast Cancer. *Mol. Imaging Biol.* **2018**, *20*, 428–435. [[CrossRef](#)] [[PubMed](#)]
20. Guo, P.; Huang, J.; Wang, L.; Jia, D.; Yang, J.; Dillon, D.A.; Zurakowski, D.; Mao, H.; Moses, M.A.; Auguste, D.T. ICAM-1 as a Molecular Target for Triple Negative Breast Cancer. *Proc. Natl. Acad. Sci. USA* **2014**, *111*, 14710–14715. [[CrossRef](#)] [[PubMed](#)]
21. Pang, B.; Zhao, Y.; Luehmann, H.; Yang, X.; Detering, L.; You, M.; Zhang, C.; Zhang, L.; Li, Z.Y.; Ren, Q.; et al. <sup>64</sup>Cu-Doped PdCu@Au Tripods: A Multifunctional Nanomaterial for Positron Emission Tomography and Image-Guided Photothermal Cancer Treatment. *ACS Nano* **2016**, *10*, 3121–3131. [[CrossRef](#)] [[PubMed](#)]
22. Ndagi, U.; Mhlongo, N.; Soliman, M.E. Metal Complexes in Cancer Therapy—An Update from Drug Design Perspective. *Drug Des. Dev. Ther.* **2017**, *11*, 599–616. [[CrossRef](#)] [[PubMed](#)]
23. Wang, D.; Lippard, S.J. Cellular Processing of Platinum Anticancer Drugs. *Nat. Rev. Drug Discov.* **2005**, *4*, 307–320. [[CrossRef](#)] [[PubMed](#)]
24. Birkbak, N.J.; Wang, Z.C.; Kim, J.Y.; Eklund, A.C.; Li, Q.; Tian, R.; Bowman-Colin, C.; Li, Y.; Greene-Colozzi, A.; Iglehart, J.D.; et al. Telomeric Allelic Imbalance Indicates Defective DNA Repair and Sensitivity to DNA-Damaging Agents. *Cancer Discov.* **2012**, *2*, 366–375. [[CrossRef](#)] [[PubMed](#)]
25. Silver, D.P.; Richardson, A.L.; Eklund, A.C.; Wang, Z.C.; Szallasi, Z.; Li, Q.; Juul, N.; Leong, C.O.; Calogrias, D.; Buraimoh, A.; et al. Efficacy of Neoadjuvant Cisplatin in Triple-Negative Breast Cancer. *J. Clin. Oncol.* **2010**, *28*, 1145–1153. [[CrossRef](#)] [[PubMed](#)]
26. Ciarimboli, G. Membrane Transporters as Mediators of Cisplatin Side-Effects. *Anticancer Res.* **2014**, *34*, 547–550. [[CrossRef](#)] [[PubMed](#)]
27. Dam, D.H.; Culver, K.S.; Odom, T.W. Grafting Aptamers onto Gold Nanostars Increases in vitro Efficacy in a Wide Range of Cancer Cell Types. *Mol. Pharm.* **2014**, *11*, 580–587. [[CrossRef](#)] [[PubMed](#)]
28. Wang, S.; Tian, Y.; Tian, W.; Sun, J.; Zhao, S.; Liu, Y.; Wang, C.; Tang, Y.; Ma, X.; Teng, Z.; et al. Selectively Sensitizing Malignant Cells to Photothermal Therapy Using a CD44-Targeting Heat Shock Protein 72 Depletion Nanosystem. *ACS Nano* **2016**, *10*, 8578–8590. [[CrossRef](#)] [[PubMed](#)]
29. Ou, Y.C.; Webb, J.A.; Faley, S.; Shae, D.; Talbert, E.M.; Lin, S.; Cutright, C.C.; Wilson, J.T.; Bellan, L.M.; Bardhan, R. Gold Nanoantenna-Mediated Photothermal Drug Delivery from Thermosensitive Liposomes in Breast Cancer. *ACS Omega* **2016**, *1*, 234–243. [[CrossRef](#)] [[PubMed](#)]
30. Santiago, T.; DeVaux, R.S.; Kurzatowska, K.; Espinal, R.; Herschkowitz, J.I.; Hepel, M. Surface-Enhanced Raman Scattering Investigation of Targeted Delivery and Controlled Release of Gemcitabine. *Int. J. Nanomed.* **2017**, *12*, 7763–7776. [[CrossRef](#)] [[PubMed](#)]
31. Saw, W.S.; Ujihara, M.; Chong, W.Y.; Voon, S.H.; Imae, T.; Kiew, L.V.; Lee, H.B.; Sim, K.S.; Chung, L.Y. Size-Dependent Effect of Cystine/Citric Acid-Capped Confeito-Like Gold Nanoparticles on Cellular Uptake and Photothermal Cancer Therapy. *Colloids Surf. B Biointerfaces* **2018**, *161*, 365–374. [[CrossRef](#)] [[PubMed](#)]

32. Ayala-Orozco, C.; Urban, C.; Bishnoi, S.; Urban, A.; Charron, H.; Mitchell, T.; Shea, M.; Nanda, S.; Schiff, R.; Halas, N.; et al. Sub-100 nm Gold Nanomatryoshkas Improve Photo-Thermal Therapy Efficacy in Large and Highly Aggressive Triple Negative Breast Tumors. *J. Control. Release* **2014**, *191*, 90–97. [[CrossRef](#)] [[PubMed](#)]
33. Kong, T.; Zeng, J.; Wang, X.; Yang, X.; Yang, J.; McQuarrie, S.; McEwan, A.; Roa, W.; Chen, J.; Xing, J.Z. Enhancement of Radiation Cytotoxicity in Breast-Cancer Cells by Localized Attachment of Gold Nanoparticles. *Small* **2008**, *4*, 1537–1543. [[CrossRef](#)] [[PubMed](#)]
34. Dube, E.; Oluwole, D.O.; Nwaji, N.; Nyokong, T. Glycosylated Zinc Phthalocyanine-Gold Nanoparticle Conjugates for Photodynamic Therapy: Effect of Nanoparticle Shape. *Spectrochim. Acta A Mol. Biomol. Spectrosc.* **2018**, *203*, 85–95. [[CrossRef](#)] [[PubMed](#)]
35. Dozie-Nwachukwu, S.O.; Obayemi, J.D.; Danyuo, Y.; Anuku, N.; Odusanya, O.S.; Malatesta, K.; Soboyejo, W.O. A Comparative Study of the Adhesion of Biosynthesized Gold and Conjugated Gold/Prodigosin Nanoparticles to Triple Negative Breast Cancer Cells. *J. Mater. Sci. Mater. Med.* **2017**, *28*, 143. [[CrossRef](#)] [[PubMed](#)]
36. Wang, C.; Jiang, Y.; Li, X.; Hu, L. Thioglucose-Bound Gold Nanoparticles Increase the Radiosensitivity of a Triple-Negative Breast Cancer Cell Line (MDA-MB-231). *Breast Cancer* **2015**, *22*, 413–420. [[CrossRef](#)] [[PubMed](#)]
37. Zhang, M.; Kim, H.S.; Jin, T.; Woo, J.; Piao, Y.J.; Moon, W.K. Near-Infrared Photothermal Therapy Using Anti-EGFR-Gold Nanorod Conjugates for Triple Negative Breast Cancer. *Oncotarget* **2017**, *8*, 86566–86575. [[CrossRef](#)] [[PubMed](#)]
38. Zhang, M.; Kim, H.S.; Jin, T.; Moon, W.K. Near-Infrared Photothermal Therapy Using EGFR-Targeted Gold Nanoparticles Increases Autophagic Cell Death in Breast Cancer. *J. Photochem. Photobiol. B.* **2017**, *170*, 58–64. [[CrossRef](#)] [[PubMed](#)]
39. Malik, M.T.; O'Toole, M.G.; Casson, L.K.; Thomas, S.D.; Bardi, G.T.; Reyes-Reyes, E.M.; Ng, C.K.; Kang, K.A.; Bates, P.J. AS1411-Conjugated Gold Nanospheres and Their Potential for Breast Cancer Therapy. *Oncotarget* **2015**, *6*, 22270–22281. [[CrossRef](#)] [[PubMed](#)]
40. Haynes, B.; Zhang, Y.; Liu, F.; Li, J.; Petit, S.; Kothayer, H.; Bao, X.; Westwell, A.D.; Mao, G.; Shekhar, M.P.V. Gold Nanoparticle Conjugated Rad6 Inhibitor Induces Cell Death in Triple Negative Breast Cancer Cells by Inducing Mitochondrial Dysfunction and PARP-1 Hyperactivation: Synthesis and Characterization. *Nanomedicine* **2016**, *12*, 745–757. [[CrossRef](#)] [[PubMed](#)]
41. Conde, J.; Oliva, N.; Artzi, N. Implantable Hydrogel Embedded Dark-Gold Nanoswitch as a Theranostic Probe to Sense and Overcome Cancer Multidrug Resistance. *Proc. Natl. Acad. Sci. USA* **2015**, *112*, E1278–E1287. [[CrossRef](#)] [[PubMed](#)]
42. Ayala-Orozco, C.; Urban, C.; Knight, M.W.; Urban, A.S.; Neumann, O.; Bishnoi, S.W.; Mukherjee, S.; Goodman, A.M.; Charron, H.; Mitchell, T.; et al. Au Nanomatryoshkas as Efficient Near-Infrared Photothermal Transducers for Cancer Treatment: Benchmarking Against Nanoshells. *ACS Nano* **2014**, *8*, 6372–6381. [[CrossRef](#)] [[PubMed](#)]
43. Yang, Z.; Liu, T.; Xie, Y.; Sun, Z.; Liu, H.; Lin, J.; Liu, C.; Mao, Z.W.; Nie, S. Chitosan Layered Gold Nanorods as Synergistic Therapeutics for Photothermal Ablation and Gene Silencing in Triple-Negative Breast Cancer. *Acta Biomater.* **2015**, *25*, 194–204. [[CrossRef](#)] [[PubMed](#)]
44. Sarkar, S.; Konar, S.; Prasad, P.N.; Rajput, S.; Kumar, B.N.P.; Rao, R.R.; Pathak, A.; Fisher, P.B.; Mandal, M. Micellar Gold Nanoparticles as Delivery Vehicles for Dual Tyrosine Kinase Inhibitor ZD6474 for Metastatic Breast Cancer Treatment. *Langmuir* **2017**, *33*, 7649–7659. [[CrossRef](#)] [[PubMed](#)]
45. Atkinson, R.L.; Zhang, M.; Diagaradjane, P.; Peddibhotla, S.; Contreras, A.; Hilsenbeck, S.G.; Woodward, W.A.; Krishnan, S.; Chang, J.C.; Rosen, J.M. Thermal Enhancement with Optically Activated Gold Nanoshells Sensitizes Breast Cancer Stem Cells to Radiation Therapy. *Sci. Transl. Med.* **2010**, *2*. [[CrossRef](#)] [[PubMed](#)]
46. Zhao, N.; Yang, Z.; Li, B.; Meng, J.; Shi, Z.; Li, P.; Fu, S. RGD-Conjugated Mesoporous Silica-Encapsulated Gold Nanorods Enhance the Sensitization of Triple-Negative Breast Cancer to Megavoltage Radiation Therapy. *Int. J. Nanomed.* **2016**, *11*, 5595–5610. [[CrossRef](#)] [[PubMed](#)]
47. Lee, J.; Chatterjee, D.K.; Lee, M.H.; Krishnan, S. Gold Nanoparticles in Breast Cancer Treatment: Promise and Potential Pitfalls. *Cancer Lett.* **2014**, *347*, 46–53. [[CrossRef](#)] [[PubMed](#)]

48. Klassen, N.V.; Kedrov, V.V.; Ossipyan, Y.A.; Shmurak, S.Z.; Shmyt Ko, I.M.; Krivko, O.A.; Kudrenko, E.A.; Kurlov, V.N.; Kobelev, N.P.; Kiselev, A.P.; et al. Nanoscintillators for Microscopic Diagnostics of Biological and Medical Objects and Medical Therapy. *IEEE Trans. Nanobiosci.* **2009**, *8*, 20–32. [[CrossRef](#)] [[PubMed](#)]
49. Fan, L.; Tian, M.; Liu, Y.; Deng, Y.; Liao, Z.; Xu, J. Salicylate •Phenanthroline Copper (II) Complex Induces Apoptosis in Triple-Negative Breast Cancer Cells. *Oncotarget* **2017**, *8*, 29823–29832. [[CrossRef](#)] [[PubMed](#)]
50. Afrasiabi, Z.; Stovall, P.; Finley, K.; Choudhury, A.; Barnes, C.; Ahmad, A.; Sarkar, F.; Vyas, A.; Padhye, S. Targeting Triple Negative Breast Cancer Cells by N3-Substituted 9,10-Phenanthrenequinone Thiosemicarbazones and Their Metal Complexes. *Spectrochim. Acta A Mol. Biomol. Spectrosc.* **2013**, *114*, 114–119. [[CrossRef](#)] [[PubMed](#)]
51. Ahir, M.; Bhattacharya, S.; Karmakar, S.; Mukhopadhyay, A.; Mukherjee, S.; Ghosh, S.; Chattopadhyay, S.; Patra, P.; Adhikary, A. Tailored-CuO-Nanowire Decorated with Folic Acid Mediated Coupling of the Mitochondrial-ROS Generation and miR425-PTEN Axis in Furnishing Potent Anti-Cancer Activity in Human Triple Negative Breast Carcinoma Cells. *Biomaterials* **2016**, *76*, 115–132. [[CrossRef](#)] [[PubMed](#)]
52. Frik, M.; Martínez, A.; Elie, B.T.; Gonzalo, O.; Ramírez de Mingo, D.; Sanaú, M.; Sánchez-Delgado, R.; Sadhukha, T.; Prabha, S.; Ramos, J.W.; et al. In Vitro and in Vivo Evaluation of Water-Soluble Iminophosphorane Ruthenium(II) Compounds. A Potential Chemotherapeutic Agent for Triple Negative Breast Cancer. *J. Med. Chem.* **2014**, *57*, 9995–10012. [[CrossRef](#)] [[PubMed](#)]
53. Irace, C.; Misso, G.; Capuozzo, A.; Piccolo, M.; Riccardi, C.; Luchini, A.; Caraglia, M.; Paduano, L.; Montesarchio, D.; Santamaria, R. Antiproliferative Effects of Ruthenium-Based Nucleolipidic Nanoaggregates in Human Models of Breast Cancer in Vitro: Insights into Their Mode of Action. *Sci. Rep.* **2017**, *7*, 45236. [[CrossRef](#)] [[PubMed](#)]
54. Nhugeaw, T.; Temboot, P.; Hansongnern, K.; Ratanaphan, A. Cellular Responses of BRCA1-Defective and Triple-Negative Breast Cancer Cells and in Vitro BRCA1 Interactions Induced by Metallo-Intercalator Ruthenium(II) Complexes Containing Chloro-Substituted Phenylazopyridine. *BMC Cancer* **2014**, *14*, 73. [[CrossRef](#)] [[PubMed](#)]
55. Montani, M.; Pazmay, G.V.B.; Hysi, A.; Lupidi, G.; Pettinari, R.; Gambini, V.; Tilio, M.; Marchetti, F.; Pettinari, C.; Ferraro, S.; et al. The Water Soluble Ruthenium(II) Organometallic Compound [Ru(p-cymene)(bis(3,5 dimethylpyrazol-1-yl)methane)Cl]Cl Suppresses Triple Negative Breast Cancer Growth by Inhibiting Tumor Infiltration of Regulatory T Cells. *Pharmacol. Res.* **2016**, *107*, 282–290. [[CrossRef](#)] [[PubMed](#)]
56. Beauperin, M.; Top, S.; Richard, M.A.; Plazuk, D.; Pigeon, P.; Toma, S.; Poláčková, V.; Jaouen, G. The Length of the Bridging Chain in Ansa-Metallocenes Influences Their Antiproliferative Activity Against Triple Negative Breast Cancer Cells (TNBC). *Dalton Trans.* **2016**, *45*, 13126–13134. [[CrossRef](#)] [[PubMed](#)]
57. Biancalana, L.; Zacchini, S.; Ferri, N.; Lupo, M.G.; Pampaloni, G.; Marchetti, F. Tuning the Cytotoxicity of Ruthenium(II) Para-Cymene Complexes by Mono-Substitution at a Triphenylphosphine/Phenoxydiphenylphosphine Ligand. *Dalton Trans.* **2017**, *46*, 16589–16604. [[CrossRef](#)] [[PubMed](#)]
58. Becceneri, A.B.; Popolin, C.P.; Plutin, A.M.; Maistro, E.L.; Castellano, E.E.; Batista, A.A.; Cominetti, M.R. The Trans-[Ru(PPh3)2(N,N-dimethyl-N'-thiophenylthioureato-k2O,S)(bipy)]PF6 Complex Has Pro-Apoptotic Effects on Triple Negative Breast Cancer Cells and Presents Low Toxicity in Vivo. *J. Inorg Biochem.* **2018**, *186*, 70–84. [[CrossRef](#)] [[PubMed](#)]
59. Popolin, C.P.; Reis, J.P.B.; Becceneri, A.B.; Graminha, A.E.; Almeida, M.A.P.; Corrêa, R.S.; Colina-Vegas, L.A.; Ellena, J.; Batista, A.A.; Cominetti, M.R. Cytotoxicity and Anti-Tumor Effects of New Ruthenium Complexes on Triple Negative Breast Cancer Cells. *PLoS ONE* **2017**, *12*, e0183275. [[CrossRef](#)] [[PubMed](#)]
60. Chen, H.; Burnett, J.; Zhang, F.; Zhang, J.; Paholak, H.; Sun, D. Highly Crystallized Iron Oxide Nanoparticles as Effective and Biodegradable Mediators for Photothermal Cancer Therapy. *J. Mater. Chem. B* **2014**, *2*, 757–765. [[CrossRef](#)]
61. Paholak, H.J.; Stevers, N.O.; Chen, H.; Burnett, J.P.; He, M.; Korkaya, H.; McDermott, S.P.; Deol, Y.; Clouthier, S.G.; Luther, T.; et al. Elimination of Epithelial-Like and Mesenchymal-Like Breast Cancer Stem Cells to Inhibit Metastasis Following Nanoparticle-Mediated Photothermal Therapy. *Biomaterials* **2016**, *104*, 145–157. [[CrossRef](#)] [[PubMed](#)]
62. Manigandan, A.; Handi, V.; Sundaramoorthy, N.S.; Dhandapani, R.; Radhakrishnan, J.; Sethuraman, S.; Subramanian, A. Responsive Nanomicellar Theranostic Cages for Metastatic Breast Cancer. *Bioconjug. Chem.* **2018**, *29*, 275–286. [[CrossRef](#)] [[PubMed](#)]

63. Xie, W.; Gao, Q.; Guo, Z.; Wang, D.; Gao, F.; Wang, X.; Wei, Y.; Zhao, L. Injectable and Self-Healing Thermosensitive Magnetic Hydrogel for Asynchronous Control Release of Doxorubicin and Docetaxel to Treat Triple-Negative Breast Cancer. *ACS Appl. Mater. Interfaces* **2017**, *9*, 33660–33673. [[CrossRef](#)] [[PubMed](#)]
64. Harmon, T.; Harbuzariu, A.; Lanier, V.; Lipsey, C.C.; Kirilin, W.; Yang, L.; Gonzalez-Perez, R.R. Nanoparticle-Linked Antagonist for Leptin Signaling Inhibition in Breast Cancer. *World J. Clin. Oncol.* **2017**, *8*, 54–66. [[CrossRef](#)] [[PubMed](#)]
65. Vyas, D.; Lopez-Hisijos, N.; Gandhi, S.; El-Dakdouki, M.; Basson, M.D.; Walsh, M.F.; Huang, X.; Vyas, A.K.; Chaturvedi, L.S. Doxorubicin-Hyaluronan Conjugated Super-Paramagnetic Iron Oxide Nanoparticles (DOX-HA-SPION) Enhanced Cytoplasmic Uptake of Doxorubicin and Modulated Apoptosis, IL-6 Release and NF-KappaB Activity in Human MDA-MB-231 Breast Cancer Cells. *J. Nanosci. Nanotechnol.* **2015**, *15*, 6413–6422. [[CrossRef](#)] [[PubMed](#)]
66. Swanner, J.; Mims, J.; Carroll, D.L.; Akman, S.A.; Furdui, C.M.; Torti, S.V.; Singh, R.N. Differential Cytotoxic and Radiosensitizing Effects of Silver Nanoparticles on Triple-Negative Breast Cancer and Non-Triple-Negative Breast Cells. *Int. J. Nanomed.* **2015**, *10*, 3937–3953. [[CrossRef](#)]
67. Juarez-Moreno, K.; Gonzalez, E.B.; Girón-Vazquez, N.; Chávez-Santoscoy, R.A.; Mota-Morales, J.D.; Perez-Mozqueda, L.L.; Garcia-Garcia, M.R.; Pestryakov, A.; Bogdanchikova, N. Comparison of Cytotoxicity and Genotoxicity Effects of Silver Nanoparticles on Human Cervix and Breast Cancer Cell Lines. *Hum. Exp. Toxicol.* **2017**, *36*, 931–948. [[CrossRef](#)] [[PubMed](#)]
68. Hearn, J.M.; Hughes, G.M.; Romero-Canelón, I.; Munro, A.F.; Rubio-Ruiz, B.; Liu, Z.; Carragher, N.O.; Sadler, P.J. Pharmaco-Genomic Investigations of Organo-Iridium Anticancer Complexes Reveal Novel Mechanism of Action. *Metallomics* **2018**, *10*, 93–107. [[CrossRef](#)] [[PubMed](#)]
69. Yang, G.J.; Zhong, H.J.; Ko, C.N.; Wong, S.Y.; Vellaisamy, K.; Ye, M.; Ma, D.L.; Leung, C.H. Identification of a Rhodium(III) Complex as a Wee1 Inhibitor Against TP53-Mutated Triple-Negative Breast Cancer Cells. *Chem. Commun.* **2018**, *54*, 2463–2466. [[CrossRef](#)] [[PubMed](#)]
70. Mooney, R.; Roma, L.; Zhao, D.; van Haute, D.; Garcia, E.; Kim, S.U.; Annala, A.J.; Aboody, K.S.; Berlin, J.M. Neural Stem Cell-Mediated Intratumoral Delivery of Gold Nanorods Improves Photothermal Therapy. *ACS Nano* **2014**, *8*, 12450–12460. [[CrossRef](#)] [[PubMed](#)]
71. Lacroix, M.; Leclercq, G. Relevance of Breast Cancer Cell Lines as Models for Breast Tumours: An Update. *Breast Cancer Res. Treat.* **2004**, *83*, 249–289. [[CrossRef](#)] [[PubMed](#)]
72. Holliday, D.L.; Speirs, V. Choosing the Right Cell Line for Breast Cancer Research. *Breast Cancer Res.* **2011**, *13*, 215. [[CrossRef](#)] [[PubMed](#)]
73. Rock, K.L.; Kono, H. The Inflammatory Response to Cell Death. *Annu. Rev. Pathol.* **2008**, *3*, 99–126. [[CrossRef](#)] [[PubMed](#)]
74. Mammucari, C.; Rizzuto, R. Signaling Pathways in Mitochondrial Dysfunction and Aging. *Mech. Ageing Dev.* **2010**, *131*, 536–543. [[CrossRef](#)] [[PubMed](#)]
75. Sohur, U.S.; Dixit, M.N.; Chen, C.L.; Byrom, M.W.; Kerr, L.A. Rel/NF-KappaB Represses Bcl-2 Transcription in Pro-B Lymphocytes. *Gene Expr.* **1999**, *8*, 219–229. [[PubMed](#)]
76. Selvakannan, P.R.; Mandal, S.; Pasricha, R.; Adyanthaya, S.D.; Sastry, M. One-Step Synthesis of Hydrophobized Gold Nanoparticles of Controllable Size by the Reduction of Aqueous Chloroaurate Ions by Hexadecylaniline at the Liquid-Liquid Interface. *Chem. Commun.* **2002**, *13*, 1334–1335. [[CrossRef](#)]
77. Okitsu, K.; Yue, A.; Tanabe, S.; Matsumoto, H.; Yobiko, Y. Formation of Colloidal Gold Nanoparticles in an Ultrasonic Field: Control of Rate of Gold (III) Reduction and Size of Formed Gold Particles. *Langmuir* **2001**, *17*, 7717–7720. [[CrossRef](#)]
78. Korbekandi, H.; Ashari, Z.; Iravani, S.; Abbasi, S. Optimization of Biological Synthesis of Silver Nanoparticles Using *Fusarium Oxysporum*. *Iran J. Pharm. Res.* **2013**, *12*, 289–298. [[PubMed](#)]
79. Iravani, S.; Korbekandi, H.; Mirmohammadi, S.V.; Zolfaghari, B. Synthesis of Silver Nanoparticles: Chemical, Physical and Biological Methods. *Res. Pharm. Sci.* **2014**, *9*, 385–406. [[PubMed](#)]
80. Lesniak, A.; Kilinc, D.; Rashdan, S.A.; von Kriegsheim, A.; Ashall, B.; Zerulla, D.; Kolch, W.; Lee, G.U. In Vitro Study of the Interaction of Heregulin-Functionalized Magnetic-Optical Nanorods with MCF7 and MDA-MB-231 Cells. *Faraday Discuss.* **2014**, *175*, 189–201. [[CrossRef](#)] [[PubMed](#)]
81. Greish, K. Enhanced Permeability and Retention (EPR) Effect for Anticancer Nanomedicine Drug Targeting. *Methods Mol. Biol.* **2010**, *624*, 25–37. [[CrossRef](#)] [[PubMed](#)]

82. Matsumura, Y.; Maeda, H. A New Concept for Macromolecular Therapeutics in Cancer Hemotherapy: Mechanism of Tumorotropic Accumulation of Proteins and the Antitumor Agent Smancs. *Cancer Res.* **1986**, *46*, 6387–6392. [[PubMed](#)]
83. Maeda, H.; Wu, J.; Sawa, T.; Matsumura, Y.; Hori, K. Tumor Vascular Permeability and the EPR Effect in Macromolecular Therapeutics: A Review. *J. Control. Release* **2000**, *65*, 271–284. [[CrossRef](#)]
84. Dam, D.H.; Culver, K.S.; Kandela, I.; Lee, R.C.; Chandra, K.; Lee, H.; Mantis, C.; Ugolkov, A.; Mazar, A.P.; Odom, T.W. Biodistribution and in Vivo Toxicity of Aptamer-Loaded Gold Nanostars. *Nanomedicine* **2015**, *11*, 671–679. [[CrossRef](#)] [[PubMed](#)]
85. Cioce, M.; Gherardi, S.; Viglietto, G.; Strano, S.; Blandino, G.; Muti, P.; Ciliberto, G. Mammosphere-Forming Cells from Breast Cancer Cell Lines as a Tool for the Identification of CSC-Like- and Early Progenitor-Targeting Drugs. *Cell Cycle* **2010**, *9*, 2878–2887. [[CrossRef](#)] [[PubMed](#)]
86. Rosen, J.M.; Jordan, C.T. The Increasing Complexity of the Cancer Stem Cell Paradigm. *Science* **2009**, *324*, 1670–1673. [[CrossRef](#)] [[PubMed](#)]
87. Bravo-Cordero, J.J.; Hodgson, L.; Condeelis, J. Directed Cell Invasion and Migration during Metastasis. *Curr. Opin. Cell Biol.* **2012**, *24*, 277–283. [[CrossRef](#)] [[PubMed](#)]
88. Anampa, J.; Sparano, J.A. New Agents for the Management of Resistant Metastatic Breast Cancer. *Expert Opin. Pharmacother.* **2017**, *18*, 1815–1831. [[CrossRef](#)] [[PubMed](#)]
89. Toraya-Brown, S.; Sheen, M.R.; Zhang, P.; Chen, L.; Baird, J.R.; Demidenko, E.; Turk, M.J.; Hoopes, P.J.; Conejo-Garcia, J.R.; Fiering, S. Local Hyperthermia Treatment of Tumors Induces CD8(+) T Cell-Mediated Resistance Against Distal and Secondary Tumors. *Nanomedicine* **2014**, *10*, 1273–1285. [[CrossRef](#)] [[PubMed](#)]
90. Aggarwal, B.B.; Shishodia, S.; Sandur, S.K.; Pandey, M.K.; Sethi, G. Inflammation and Cancer: How Hot Is the Link? *Biochem. Pharmacol.* **2006**, *72*, 1605–1621. [[CrossRef](#)] [[PubMed](#)]
91. Salgado, R.; Junius, S.; Benoy, I.; van Dam, P.; Vermeulen, P.; van Marck, E.; Huget, P.; Dirix, L.Y. Circulating Interleukin-6 Predicts Survival in Patients with Metastatic Breast Cancer. *Int. J. Cancer* **2003**, *103*, 642–646. [[CrossRef](#)] [[PubMed](#)]
92. Berberoglu, U.; Yildirim, E.; Celen, O. Serum Levels of Tumor Necrosis Factor Alpha Correlate with Response to Neoadjuvant Chemotherapy in Locally Advanced Breast Cancer. *Int. J. Biol. Markers* **2004**, *19*, 130–134. [[CrossRef](#)] [[PubMed](#)]
93. Hartmann, L.C.; Keeney, G.L.; Lingle, W.L.; Christianson, T.J.; Varghese, B.; Hillman, D.; Oberg, A.L.; Low, P.S. Folate Receptor Overexpression Is Associated with Poor Outcome in Breast Cancer. *Int. J. Cancer* **2007**, *121*, 938–942. [[CrossRef](#)] [[PubMed](#)]



© 2018 by the authors. Licensee MDPI, Basel, Switzerland. This article is an open access article distributed under the terms and conditions of the Creative Commons Attribution (CC BY) license (<http://creativecommons.org/licenses/by/4.0/>).